

astro-ph/0301505  
 U M N {T H {2127/03  
 T P I{M INN {03/02  
 January 2003

## TA S I L E C T U R E S O N D A R K M A T T E R

K E I T H A . O L I V E <sup>Y</sup>

W illiam I. F ine T heoretical P hysics I nstitute, S chool of P hysics and A stronom y,  
 U niversity of M innesota, M inneapolis, M N 55455 U SA  
 E -m ail: olive@ um n.edu

O bservational evidence and theoretical m otivation for dark m atter are presented and connections to the CMB and BBN are m ade. P roblems for baryonic and neutrino dark m atter are sum m arized. Em phasis is placed on the prospects for supersym m etric dark m atter.

### 1. Lecture 1

The nature and identity of the dark m atter of the U niverse is one of the m ost challenging problem s facing m odern cosm ology. The problem is a long-standing one, going back to early observations of mass-to-light ratios by Zwicky<sup>1</sup>. Given the distribution (by number) of galaxies w ith total lum inosity  $L$ ,  $\langle L \rangle$ , one can compute the mean lum inosity density of galaxies

$$Z = \frac{1}{\langle L \rangle} \int L dL \quad (1)$$

w hich is determined to be<sup>2</sup>

$$L' = 2 \times 10^2 h_0 L \text{ M pc}^3 \quad (2)$$

w here  $L' = 3.8 \times 10^3 \text{ erg s}^{-1}$  is the solar lum inosity. In the absence of a cosm ological constant, one can define a critical energy density,  $\rho_c = 3H^2/8\pi G_N = 1.88 \times 10^{-29} h_0^2 \text{ g cm}^{-3}$ , such that  $\rho = \rho_c$  for three-space curvature  $k = 0$ , w here the present value of the Hubble parameter has been defined by  $H_0 = 100h_0 \text{ km M pc}^{-1} \text{ s}^{-1}$ . We can now define a critical mass-to-light ratio is given by

$$(M/L)_c = \rho_c / L' = 1390 h_0 (M/L) \quad (3)$$

---

<sup>1</sup>Summary of lectures given at the T heoretical A dvanced Study I nstitute in E lementary P article P hysics at the U niversity of C olorado at B oulder - June 2-28, 2002.

<sup>2</sup>This work w as supported in part by D O E grant D E -F G 02-94ER 40823 at M innesota.

which can be used to determine the cosmological density parameter

$$\Omega = \frac{M}{c^2} = (M/L) = (M/L)_c \quad (4)$$

Mass-to-light ratios are, however, strongly dependent on the distance scale on which they are determined<sup>3</sup>. In the solar neighborhood  $M/L \approx 2-1$  (in solar units), yielding values of  $\Omega$  of only  $\approx 0.01$ . In the bright central parts of galaxies,  $M/L \approx (10-20)h$ , so that  $\Omega \approx 0.01$ . On larger scales, that of binaries and small groups of galaxies,  $M/L \approx (60-180)h$  and  $\Omega \approx 0.1$ . On even larger scales, that of clusters,  $M/L$  may be as large as  $(200-500)h$ , giving  $\Omega \approx 0.3$ . This progression in  $M/L$  seems to have halted, as even on the largest scales observed today, mass-to-light ratios imply values of  $\Omega < 0.3-0.4$ . Thus when one considers the scale of galaxies (and their halos) and larger, the presence of dark matter (and as we shall see, non-baryonic dark matter) is required.

Direct observational evidence for dark matter is found from a variety of sources. On the scale of galactic halos, the observed flatness of the rotation curves of spiral galaxies is a clear indicator for dark matter. There is also evidence for dark matter in elliptical galaxies, as well as clusters of galaxies coming from the X-ray observations of these objects. Also, direct evidence has been obtained through the study of gravitational lenses. On the theoretical side, we predict the presence of dark matter (or dark energy) because 1) it is a strong prediction of most inflationary models (and there is at present no good alternative to inflation) and 2) our current understanding of galaxy formation requires substantial amounts of dark matter to account for the growth of density fluctuations. One can also make a strong case for the existence of non-baryonic dark matter in particular. The recurrent problem with baryonic dark matter is that not only is it very difficult to hide baryons, but given the amount of dark matter required on large scales, there is a direct conflict with primordial nucleosynthesis if all of the dark matter is baryonic. In this first lecture, I will review the observational and theoretical evidence supporting the existence of dark matter.

### 1.1. Observational Evidence

Assuming that galaxies are in virial equilibrium, one expects that one can relate the mass at a given distance  $r$ , from the center of a galaxy to its rotational velocity by

$$M(r) / v^2 r = G_N \quad (5)$$

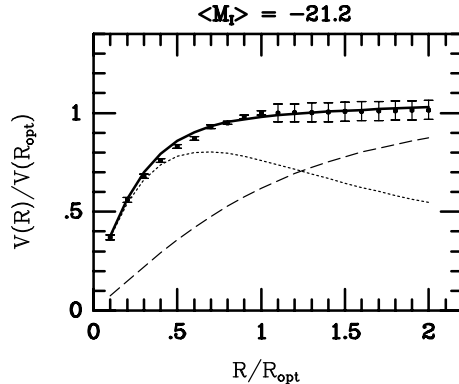


Figure 1. Synthetic rotation curve<sup>5</sup> for galaxies with  $\langle M_i \rangle = -21.2$ . The dotted curve shows the disk contribution, whereas the dashed curve shows the halo contribution.

The rotational velocity,  $v$ , is measured<sup>3,4</sup> by observing 21 cm emission lines in H I regions (neutral hydrogen) beyond the point where most of the light in the galaxy ceases. A subset of a compilation<sup>5</sup> of nearly 1000 rotation curves of spiral galaxies is shown in Fig. 1. The subset shown is restricted to a narrow range in brightness, but is characteristic for a wide range of spiral galaxies. Shown is the rotational velocity as a function of  $r$  in units of the optical radius. If the bulk of the mass is associated with light, then beyond the point where most of the light stops,  $M$  would be constant and  $v^2 / r = 1$ . This is not the case, as the rotation curves appear to be flat, i.e.,  $v$  constant outside the core of the galaxy. This implies that  $M / r$  beyond the point where the light stops. This is one of the strongest pieces of evidence for the existence of dark matter. Velocity measurements indicate dark matter in elliptical galaxies as well<sup>6</sup>.

Galactic rotation curves are not the only observational indication for the existence of dark matter. X-ray emitting hot gas in elliptical galaxies also provides an important piece of evidence for dark matter. A particularly striking example is that of the large elliptical M 87. Detailed profiles of the temperature and density of the hot X-ray emitting gas have been mapped out<sup>7</sup>. Assuming hydrostatic equilibrium, these measurements allow one to determine the overall mass distribution in the galaxy necessary to bind the hot gas. Based on an isothermal model with temperature  $kT = 3 \text{ keV}$  (which leads to a conservative estimate of the total mass), Fabricant and Gorenstein<sup>7</sup> predicted that the total mass out to a radial distance of 392 kpc is  $5.7 \times 10^{13} M_{\odot}$ , whereas the mass in the hot gas is only  $2.8 \times 10^{12} M_{\odot}$ .

or only 5% of the total. The visible mass is expected to contribute only 1% of the total.

M 87 is not the only example of an elliptical galaxy in which X-ray emitting hot gas is observed to indicate the presence of dark matter. X-ray observations have shown that the total mass associated with elliptical galaxies is considerably larger than the luminous component in many examples of varying morphological types<sup>8</sup>. Mass-to-light ratios for these systems vary, with most being larger than  $30h_0$  and some ranging as high as  $200h_0$ .

In addition, similar inferences pertaining to the existence of dark matter can be made from the X-ray emission from small groups of galaxies<sup>9</sup>. On these scales, mass-to-light ratios are typically  $> 100h_0$  and detailed studies have shown that the baryon fraction in these systems is rather small. Furthermore, it was argued<sup>10</sup> that cluster baryon fractions should not differ from the universal value given by  $B = m$ . Using an estimate of  $B = 0.04$  from big bang nucleosynthesis (BBN, see below), and baryon fractions ranging from 0.1 to 0.3, one would obtain an estimate for the total matter density of  $0.13 \pm 0.4$ .

Another piece of evidence on large scales is available from gravitational lensing<sup>11</sup>. The systematic lensing of the roughly 150,000 galaxies per deg<sup>2</sup> at redshifts between  $z = 1 \text{ to } 3$  into arcs and arclets allow one to trace the matter distribution in a foreground cluster. Lensing observations can be categorized as either strong (multiple images) or weak (single images). Both require the presence of a dominant dark matter component.

Strong lensing is particularly adept in testing the overall geometry of the Universe<sup>12,13</sup>. While a cluster which provides multiple lenses of a single background galaxy (at known redshift) is useful for determining the total cluster mass, when several background galaxies are lensed, it is possible to constrain the values of  $m$  and  $B$ <sup>14</sup>. The recent results of<sup>13</sup> show a degeneracy in the  $m \pm B$  plane. Nevertheless, the allowed region is a set from similar types of degeneracies found in supernovae searches and the CMB (see below). Indeed, these lensing results are much more constraining in  $m$  than the other techniques, though a residual uncertainty of about 30% persists. While in principle, these results find that any value (from 0 to 1) is possible for  $m$ ,  $m < 0.5$  for low values of  $B$  and  $m < 0.4$  for higher values of  $B (> 0.6)$ .

Weak lensing of galaxies by galaxies can (on a statistical basis) also probe the nature of galactic halos. Recent studies based on weak lensing data indicate that galactic halos may be far more extended than previously thought<sup>15</sup> (radii larger than  $200 h_0^{-1} \text{ kpc}$ ). These results also imply a sub-

stantial contribution to  $\Omega_m$  (of order 0.1-0.2) on this scale. On larger scales, using many cluster lenses enables one to estimate  $\Omega_m \approx 0.3$ <sup>16</sup>. Another use of weak lensing statistics is to determine the evolution of cosmic shear and hence an estimate of  $\Omega_m$ <sup>17</sup>. Finally, there exist a number of examples of dark clusters, i.e., lenses with no observable counterpart<sup>18</sup>. The contribution of these objects (if they are robust) to  $\Omega_m$  is not clear. For a recent review of weak lensing see<sup>19</sup>.

Finally, on very large scales, it is possible to get an estimate of  $\Omega_m$  from the distribution of peculiar velocities of galaxies and clusters. On scales, where perturbations,  $\delta$ , are still small, peculiar velocities can be expressed<sup>20</sup> as  $v \approx H \Omega_m^{0.6}$ . On these scales, older measurements of the peculiar velocity field from the IRAS galaxy catalogue indicate that indeed  $\Omega_m$  is close to unity<sup>21</sup>. Some of the new data indicates a lower value in the range<sup>22</sup> 0.2 to 0.5, but does not conclusively exclude  $\Omega_m = 1$ <sup>23</sup>.

The above discussion of observational evidence for dark matter pertains largely to the overall matter density of the Universe  $\Omega_m$ . (For a comprehensive review of determinations of the matter density, see ref. <sup>24</sup>.) However, the matter density and the overall curvature are not related one-to-one. The expansion rate of the Universe in the standard FRW model is expressed by the Friedmann equation

$$H^2 = \frac{R_{,t}^2}{R^2} = \frac{8\pi G_N}{3} \Omega_m + \frac{k}{R^2} + \frac{\Lambda}{3} \quad (6)$$

where  $R_{,t}$  is the cosmological scale factor,  $k$  is the three-space curvature constant ( $k = 0; +1$ ; 1 for a spatially flat, closed or open Universe), and  $\Lambda$  is the cosmological constant. The Friedmann equation can be rewritten as

$$(1 - \Lambda)H^2 = \frac{k}{R^2} \quad (7)$$

so that  $k = 0; +1$ ; 1 corresponds to  $\Lambda = 1$ ;  $\Lambda > 1$  and  $\Lambda < 1$ . However, the value of  $\Lambda$  appearing in Eq. (7) represents the sum  $\Lambda = \Omega_m + \Lambda_0$  of contributions from the matter density ( $\Omega_m$ ) and the cosmological constant ( $\Lambda_0 = -3H^2$ ).

There has been a great deal of progress in the last several years concerning the determination of both  $\Omega_m$  and  $\Lambda$ . Cosmic microwave background (CMB) anisotropy experiments have been able to determine the curvature (i.e. the sum of  $\Omega_m$  and  $\Lambda$ ) to within about 10%, while observations of type Ia supernovae at high redshift provide information on a (nearly) orthogonal combination of the two density parameters.

The CMB is of course deeply rooted in the development and verification of the big bang model<sup>25</sup>. Indeed, it was the formulation of BBN that led to the prediction of the microwave background. The argument is rather simple. BBN requires temperatures greater than 100 keV, which according to the standard model temperature relation,  $t_s T_M^2 = 2.4 \frac{p}{N}$ , where  $N$  is the number of relativistic degrees of freedom at temperature  $T$ , and corresponds to timescales less than about 200 s. The typical cross section for the first link in the nucleosynthetic chain is

$$\sigma(p + n \rightarrow D + \gamma) \approx 5 \times 10^{-20} \text{ cm}^3 \text{ s} \quad (8)$$

This implies that it was necessary to achieve a density

$$n \approx \frac{1}{vt} \approx 10^{17} \text{ cm}^{-3} \quad (9)$$

for nucleosynthesis to begin. The density in baryons today is known approximately from the density of visible matter to be  $n_B \approx 10^{-7} \text{ cm}^{-3}$  and since we know that the density scales as  $R^{-3} \approx T^3$ , the temperature today must be

$$T_0 = (n_B / n)^{1/3} T_{BBN} \approx 10 \text{ K} \quad (10)$$

thus linking two of the most important tests of the Big Bang theory.

Microwave background anisotropy measurements have made tremendous advances in the last few years. The power spectrum<sup>26,27,28</sup> has been measured relatively accurately out to multipole moments corresponding to  $l \approx 1000$ . The details of this spectrum enable one to make accurate predictions of a large number of fundamental cosmological parameters<sup>27,29,30,31,32,33</sup>. An example of these results as found by a recent frequentist analysis<sup>34</sup> is shown in Fig. 2.

Of particular interest to us here is the CMB determination of the total density,  $\rho_{tot}$ , as well as the matter density  $\rho_m$ . The results of recent CMB anisotropy measurements are summarized in Table 1. As one can see, there is strong evidence that the Universe is flat or very close to it. Furthermore, the matter density is very consistent with the observational determinations discussed above and the baryon density, as we will see below, is consistent with the BBN production of D/H and its abundance in quasar absorption systems.

The discrepancy between the CMB value of  $\rho_m$  and  $\rho_B$  is a sign that non-baryonic matter (dark matter) is required. Furthermore, the apparent discrepancy between the CMB value of  $\rho_{tot}$  and  $\rho_m$ , though not conclusive on its own, is a sign that a contribution from the vacuum energy density or

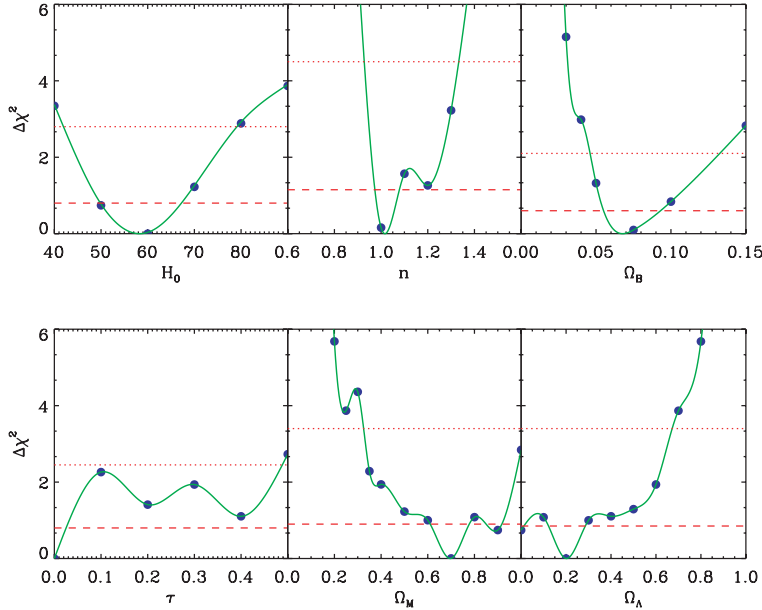


Figure 2.  $\Delta\chi^2$  calculated with the MAXIMA-1 and COBE data as a function of parameter value. Solid blue circles show grid points in parameter space, and the green lines were obtained by interpolating between grid points. The parameter values where the green line intercepts the red dashed (dotted) line corresponds to the 68% (95%) frequentist confidence region<sup>34</sup>.

Table 1. Results from recent CMB anisotropy measurements.

	tot	$m h^2$	$b h^2$
BOOMERANG <sup>27</sup>	1.03 0.06	0.12 0.05	$0.021^{+0.004}_{-0.003}$
MAXIMA <sup>29</sup>	$0.9^{+0.09}_{-0.08}$	$0.17^{+0.08}_{-0.04}$	0.0325 0.0125
MAXIMA (freq.) <sup>34</sup>	$0.89^{+0.13}_{-0.10}$	$0.25^{+0.07}_{-0.09}$	$0.026^{+0.010}_{-0.006}$
DASI <sup>30</sup>	1.04 0.06	0.14 0.04	$0.022^{+0.004}_{-0.003}$
CB <sup>31</sup>	0.99 0.12	$0.17^{+0.08}_{-0.06}$	$0.022^{+0.015}_{-0.009}$
VSA <sup>32</sup>	1.03 0.012	$0.13^{+0.08}_{-0.05}$	0.029 0.009
Archeops <sup>33</sup>	$1.16^{+0.24}_{-0.20}$	{	$0.019^{+0.006}_{-0.007}$

cosmological constant, is also required. The preferred region in the  $m$  plane as determined by a frequentist analysis of MAXIMA data is shown in Fig. 3.

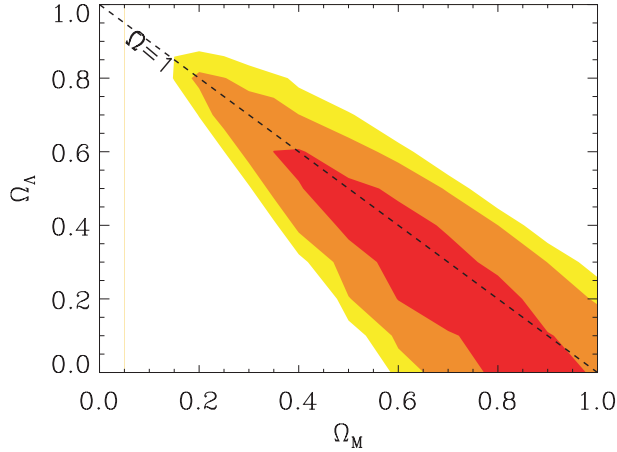


Figure 3. Two-dimensional frequentist confidence regions in the  $(\Omega_M; G_N)$  plane. The red, orange and yellow regions correspond to the 68%, 95%, and 99% confidence regions respectively. The dashed black line corresponds to a flat universe,  $\Omega_M + G_N = 1$ .

The presence or absence of a cosmological constant is a long standing problem in cosmology. To theorists, it is particularly offensive due to the necessary smallness of the constant. We know that the cosmological term is at most a factor of a few times larger than the current mass density. Thus from Eq. (6), we see that the dimensionless combination,  $G_N < 10^{-121}$ . Nevertheless, even a small non-zero value for  $\Lambda$  could greatly affect the future history of the Universe: allowing open Universes to recollapse (if  $\Lambda < 0$ ), or closed Universes to expand forever (if  $\Lambda > 0$  and sufficiently large).

Another exciting development has been the use of type Ia supernovae, which now allow measurement of relative distances with 5% precision. In combination with Cepheid data from the HST key project on the distance scale, SNe results are the dominant contributor to the best modern value for  $H_0$ :  $72 \text{ km s}^{-1} \text{Mpc}^{-1} \pm 10\%$ <sup>35</sup>. Better still, the analysis of high- $z$  SNe has allowed the first meaningful test of cosmological geometry to be carried out, as shown in Fig. 4.

These results can be contrasted with those from the CMB anisotropy measurements as in Fig. 5. We are led to a seemingly conclusive picture. The Universe is nearly flat with  $\Omega_{\text{tot}} \approx 1$ . However the density in matter makes up only 20-50% of this total, with the remainder in a cosmological constant or some other form of dark energy.

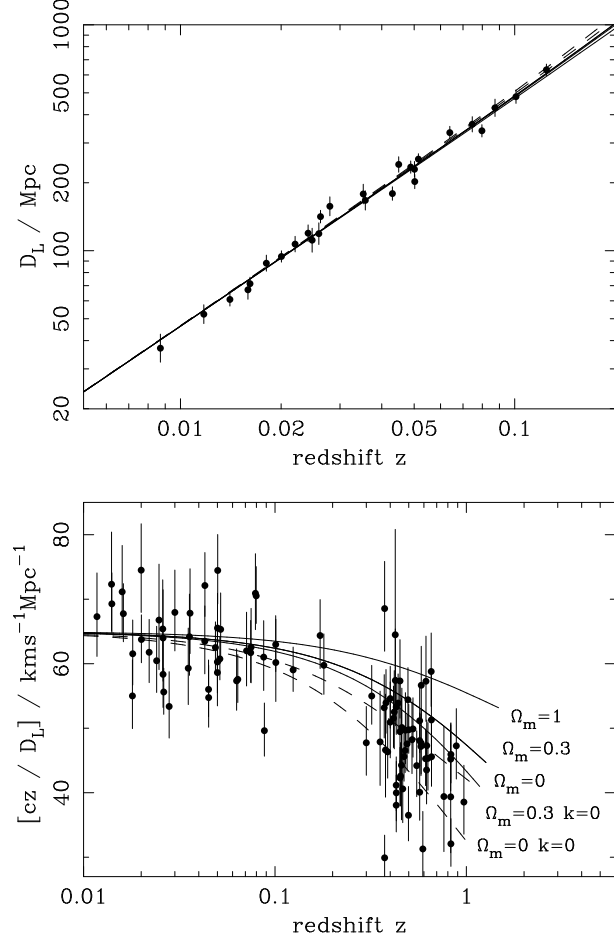


Figure 4. The type Ia supernova Hubble diagram<sup>36</sup> taken from<sup>37</sup>. The first panel shows that, for  $z < 1$ , the large-scale Hubble flow is indeed linear and uniform; the second panel shows an expanded scale, with the linear trend divided out, and with the redshift range extended to show how the Hubble law becomes nonlinear. Comparison with the prediction of Friedmann-Lemaitre models appears to favor a vacuum-dominated universe.

## 1.2. Theory

Theoretically, there is no lack of support for the dark matter hypothesis. The standard big bang model including inflation almost requires  $\Omega_{\text{tot}} = 1$ <sup>38</sup>. This can be seen from the following simple solution to the curvature problem. The simple and unfortunate fact that at present we do not even

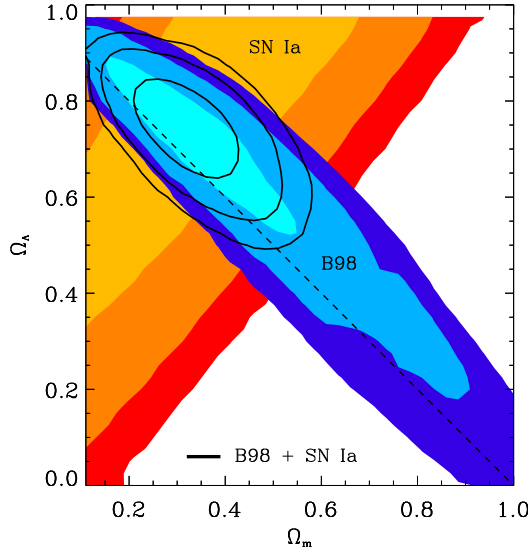


Figure 5. Likelihood-based confidence contours<sup>27</sup> over the plane (i.e.  $\nu$  assuming  $w = -1$  vs  $\Omega_m$ ). The SN Ia results very nearly constrain  $\nu \approx -1$ , whereas the results of CMB anisotropies (from the Boomerang 98 data) favor a flat model with  $\nu + \Omega_m \approx 1$ . The intersection of these constraints is the most direct (but far from the only) piece of evidence favoring a flat model with  $\Omega_m \approx 0.3$ .

know whether  $\nu$  is larger or smaller than one, indicates that we do not know the sign of the curvature term further implying that it is subdominant in Eq. (6)

$$\frac{k}{R^2} < \frac{8\pi G}{3} \quad (11)$$

In an adiabatically expanding Universe,  $R \propto T^{-1}$  where  $T$  is the temperature of the thermal photon background. Therefore the quantity

$$\hat{k} = \frac{k}{R^2 T^2} < \frac{8\pi G}{3 T_0^2} < 2 \times 10^{-58} \quad (12)$$

is dimensionless and constant in the standard model. This is known as the curvature problem and can be resolved by a period of inflation. Before inflation, let us write  $R = R_i$ ,  $T = T_i$  and  $R \propto T^{-1}$ . During inflation,  $R \propto T^{-1} e^{Ht}$ , where  $H$  is constant. After inflation,  $R = R_f = R_i$  but  $T = T_f = T_R < T_i$  where  $T_R$  is the temperature to which the Universe reheats. Thus  $R \propto T$  and  $\hat{k} \neq 0$  is not constant. But from Eqs. (7) and

(12) if  $\hat{k} \neq 0$  then  $\hat{k} \neq 1$ , and since typical inflationary models contain much more expansion than is necessary, becomes exponentially close to one.

The inflationary prediction of  $\hat{k} = 1$  is remarkably consistent with the CMB measurements discussed above. Furthermore, we know two things: Dark matter exists, since we don't see  $\hat{k} = 1$  in luminous objects, and most (about 90%) of the dark matter is not baryonic. The latter conclusion is a result of our forthcoming discussion on BBN which constrains the baryon-to-photon ratio and hence  $\hat{k}_B$ . Thus  $\hat{k}_B$  is not only dark but also non-baryonic. Furthermore, the matter density is surely composed of several contributions:  $\hat{k}_m = \hat{k}_B + \hat{k}_D + \hat{k}_M$  where the latter represents the dark matter contribution.

Another important piece of theoretical evidence for dark matter comes from the simple fact that we are living in a galaxy. The type of perturbations produced by inflation<sup>39</sup> are, in most models, adiabatic perturbations ( $\hat{k} = \hat{k}_m / T = T$ ), and I will restrict my attention to these. Indeed, the perturbations produced by inflation also have the very nearly scale-free spectrum described by Harrison and Zeldovich<sup>40</sup>. When produced, scale-free perturbations fall off as  $\hat{k} / l^2$  (increase as the square of the wave number). At early times  $\hat{k} = \hat{k}_m$  grows as  $t$  until the time when the horizon scale (which is proportional to the age of the Universe) is comparable to  $l$ . At later times, the growth halts (the mass contained within the volume  $l^3$  has become smaller than the Jean's mass) and  $\hat{k} = \hat{k}_m$  (roughly) independent of the scale  $l$ . When the Universe becomes matter dominated, the Jean's mass drops dramatically and growth continues as  $\hat{k} = \hat{k}_m / R = 1/T$ .

The transition to matter dominance is determined by setting the energy densities in radiation (photons and any massless neutrinos) equal to the energy density in matter (baryons and any dark matter). For three massless neutrinos and baryons (no dark matter), matter dominance begins at

$$T_m = 0.22 m_B \quad (13)$$

and for  $m_B < 7 \times 10^{10}$ , this corresponds to  $T_m < 0.14$  eV.

Because we are considering adiabatic perturbations, there will be anisotropies produced in the microwave background radiation on the order of  $T = T_m$ . The value of  $\hat{k}_m$ , the amplitude of the density fluctuations at horizon crossing, has been determined by COBE<sup>41</sup>,  $\hat{k}_m = (5.7 \pm 0.4) \times 10^6$ . Without the existence of dark matter,  $\hat{k}_m$  in baryons could then achieve a maximum value of only  $\hat{k}_m = A$  ( $T_m = T_0$ )  $< 2 \times 10^3 A$ , where  $T_0 = 2.35 \times 10^4$  eV is the present temperature of the microwave back-

ground and  $A = 1 \pm 10$  is a scale dependent growth factor. The overall growth in  $\delta$  is too small to argue that growth has entered a nonlinear regime needed to explain the large value ( $10^5$ ) of  $\delta$  in galaxies.

Dark matter easily remedies this dilemma in the following way. The transition to matterdominance is determined by setting equal to each other the energy densities in radiation (photons and any massless neutrinos) and matter (baryons and any dark matter). While if we suppose that there exists dark matter with an abundance  $Y = n/m$  (the ratio of the number density of 's to photons) then

$$T_m = 0.22m \cdot Y \quad (14)$$

Since we can write  $m \cdot Y = G \cdot eV = h^2 = (4 \pm 10^7)$ , we have  $T_m = T_0 = 2.4 \cdot 10^4 \cdot h^2$  which is to be compared with 600 in the case of baryons alone. The baryons, although still bound to the radiation until decoupling, now see deep potential wells formed by the dark matter perturbations to fall into and are no longer required to grow at the rate  $\delta = \dot{\delta}/R$ .

With regard to dark matter and galaxy formation, all forms of dark matter are not equal. They can be distinguished by their relative temperature at  $T_m$ <sup>42</sup>. Particles which are still largely relativistic at  $T_m$  (like neutrinos or other particles with  $m < 100 \text{ eV}$ ) have the property<sup>43</sup> that (due to free streaming) they erase perturbations out to very large scales given by the Jeans mass

$$M_J = 3 \cdot 10^{18} \frac{M}{m^2 (\text{eV})} \quad (15)$$

Thus, very large scale structures form first and galaxies are expected to fragment out later. Particles with this property are termed hot dark matter particles. Cold particles ( $m > 1 \text{ M eV}$ ) have the opposite behavior. Small scale structures form first aggregating to form larger structures later. It is now wellknown that pure HDM cosmologies can not reproduce the observed large scale structure of the Universe. In contrast, CDM does much better. Current attention is focused on so-called CDM cosmologies based on the  $m$  contribution to the curvature discussed above.

## 2. Lecture 2

### 2.1. Big Bang Nucleosynthesis

The standard model<sup>44</sup> of big bang nucleosynthesis (BBN) is based on the relatively simple idea of including an extended nuclear network into a homogeneous and isotropic cosmology. Apart from the input nuclear cross

sections, the theory contains only a single parameter, namely the baryon-to-photon ratio, . Other factors, such as the uncertainties in reaction rates, and the neutron mean-life can be treated by standard statistical and Monte Carlo techniques<sup>45,46</sup>. The theory then allows one to make predictions (with well-defined uncertainties) of the abundances of the light elements, D, <sup>3</sup>He, <sup>4</sup>He, and <sup>7</sup>Li.

### 2.1.1. Theory

Conditions for the synthesis of the light elements were attained in the early Universe at temperatures  $T > 1 \text{ MeV}$ . In the early Universe, the energy density was dominated by radiation with

$$= \frac{2}{30} \left( 2 + \frac{7}{2} + \frac{7}{4} N \right) T^4 \quad (16)$$

from the contributions of photons, electrons and positrons, and N neutrino flavors (at higher temperatures, other particle degrees of freedom should be included as well). At these temperatures, weak interaction rates were in equilibrium. In particular, the processes



fix the ratio of number densities of neutrons to protons. At  $T = 1 \text{ MeV}$ ,  $(n/p) = 1$ .

The weak interactions do not remain in equilibrium at lower temperatures. Freeze-out occurs when the weak interaction rate,  $\frac{G_F^2}{H} T^5$ , falls below the expansion rate which is given by the Hubble parameter,  $\frac{P}{G_N} = T^2 M_P$ , where  $M_P = 1 = \frac{P}{G_N} = 1.2 \times 10^9 \text{ GeV}$ . The interactions in eq. (17) freeze-out at about  $0.8 \text{ MeV}$ . As the temperature falls and approaches the point where the weak interaction rates are no longer fast enough to maintain equilibrium, the neutron to proton ratio is given approximately by the Boltzmann factor,  $(n/p) = e^{-m/T} = 1/6$ , where  $m$  is the neutron-proton mass difference. After freeze-out, free neutron decays drop the ratio slightly to about  $1/7$  before nucleosynthesis begins.

The nucleosynthesis chain begins with the formation of deuterium by the process,  $p + n \rightarrow D + \gamma$ . However, because of the large number of photons relative to nucleons,  $\gamma = n_B = 10^{10}$ , deuterium production

is delayed past the point where the temperature has fallen below the deuterium binding energy,  $E_B = 2.2 \text{ MeV}$  (the average photon energy in a blackbody is  $E \approx 2.7T$ ). This is because there are many photons in the exponential tail of the photon energy distribution with energies  $E > E_B$  despite the fact that the temperature or  $E$  is less than  $E_B$ . The degree to which deuterium production is delayed can be found by comparing the qualitative expressions for the deuterium production and destruction rates,

$$\begin{array}{ccc} p & n_B & v \\ d & n & ve^{E_B/T} \end{array} \quad (18)$$

When the quantity  $1/\exp(-E_B/T) - 1$ , the rate for deuterium destruction ( $D + p \rightarrow n + ve^{E_B/T}$ ) finally falls below the deuterium production rate and the nuclear chain begins at a temperature  $T \approx 0.1 \text{ MeV}$ .

The dominant product of big bang nucleosynthesis is  $^4\text{He}$  and its abundance is very sensitive to the  $(n/p)$  ratio

$$Y_p = \frac{2(n/p)}{[1 + (n/p)]} \quad 0.25 \quad (19)$$

i.e., an abundance of close to 25% by mass. Lesser amounts of the other light elements are produced:  $D$  and  $^3\text{He}$  at the level of about  $10^{-5}$  by number, and  $^7\text{Li}$  at the level of  $10^{-10}$  by number.

The resulting abundances of the light elements<sup>46</sup> are shown in Figure 6, over the range in  $_{10} = 10^{10}$  between 1 and 10. The left plot shows the abundance of  $^4\text{He}$  by mass,  $Y$ , and the abundances of the other three isotopes by number. The curves indicate the central predictions from BBN, while the bands correspond to the uncertainty in the predicted abundances based primarily on the uncertainty in the input nuclear reactions as computed by Monte Carlo in ref. <sup>46</sup>. This theoretical uncertainty is shown explicitly in the right panel as a function of  $_{10}$ . The dark shaded boxes correspond to the observed abundances of  $^4\text{He}$  and  $^7\text{Li}$  and will be discussed below. The dashed boxes correspond to the ranges of the elements consistent with the systematic uncertainties in the observations. The broad band shows a liberal range for  $_{10}$  consistent with the observations. At present, there is a general concordance between the theoretical predictions and the observational data.

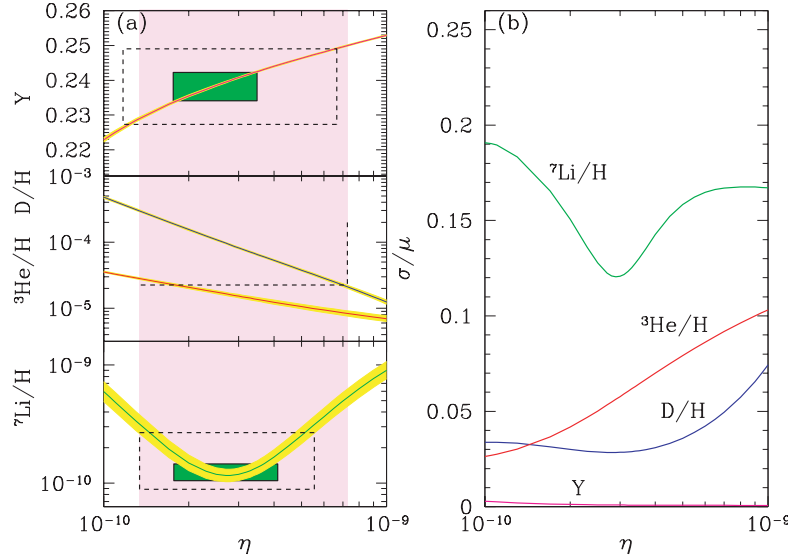


Figure 6. The light element abundances from big bang nucleosynthesis as a function of  $\eta$ .

### 2.1.2. Abundances

In addition to its BBN production,  $^4\text{He}$  is made in stars, and thus co-produced with heavy elements. Hence the best sites for determining the primordial  $^4\text{He}$  abundance are in metal-poor regions of hot, ionized gas in nearby external galaxies (extragalactic H II regions). Helium indeed shows a linear correlation with metallicity in these systems, and the extrapolation to zero metallicity gives the primordial abundance (baryonic mass fraction)<sup>47</sup>

$$Y_p = 0.238 \pm 0.002 \pm 0.005: \quad (20)$$

Here, the first error is statistical and reflects the large sample of systems, whilst the second error is systematic and dominates.

The systematic uncertainties in these observations have not been thoroughly explored to date<sup>48</sup>. In particular, there may be reason to suspect that the above primordial abundance will be increased due to effects such as underlying stellar absorption in the H II regions. We note that other analyses give similar results:  $Y_p = 0.244 \pm 0.002 \pm 0.005$ <sup>49</sup> and 0.239

0.002<sup>50</sup>.

The primordial  $^7\text{Li}$  abundance comes from measurements in the atmospheres of primitive (Population II) stars in the stellar halo of our Galaxy. The  $^7\text{Li}/\text{H}$  abundance is found to be constant for stars with low metallicity, indicating a primordial component, and a recent determination gives

$$\frac{^7\text{Li}}{\text{H}_p} = (1.23 \pm 0.06^{+0.68}_{-0.32}) \times 10^{-10} \text{ (95% CL);} \quad (21)$$

where the small statistical error is overshadowed by systematic uncertainties<sup>51</sup>. The range (21) may, however, be underestimated, as a recent determination<sup>52</sup> uses a different procedure to determine stellar atmosphere parameters, and gives  $^7\text{Li}/\text{H}_p = (2.19 \pm 0.28) \times 10^{-10}$ . At this stage, it is not possible to determine which method of analysis is more accurate, indicating the likelihood that the upper systematic uncertainty in (21) has been underestimated. Thus, in order to obtain a conservative bound from  $^7\text{Li}$ , we take the lower bound from (21) and the upper bound from<sup>52</sup>, giving

$$9.0 \times 10^{-11} < \frac{^7\text{Li}}{\text{H}_p} < 2.8 \times 10^{-10}; \quad (22)$$

D deuterium is measured in high-redshift QSO absorption line systems via its isotopic shift from hydrogen. In several absorbers of moderate column density (Lyman-limit systems), D has been observed in multiple Lyman transitions<sup>53,54</sup>. Restricting our attention to the three most reliable regions<sup>53</sup>, we find a weighted mean of

$$\frac{D}{\text{H}_p} = (2.9 \pm 0.3) \times 10^{-5}; \quad (23)$$

It should be noted, however, that the  $\chi^2$  per degree of freedom is rather poor ( $\sim 3.4$ ), and that the unweighted dispersion of these data is  $0.6 \times 10^{-5}$ . This already points to the dominance of systematic effects. Observation of D in systems with higher column density (damped systems) and lower D/H<sup>55</sup>, at a level inconsistent with (23), further suggesting that systematic effects dominate the error budget<sup>56</sup>. If all the available observations are used, we would find  $D/\text{H} = (2.6 \pm 0.3) \times 10^{-5}$  with an even worse  $\chi^2$  per degree of freedom ( $\sim 4.3$ ) and an unweighted dispersion of 0.8.

Because there are no known astrophysical sites for the production of deuterium, all observed D is assumed to be primordial<sup>57</sup>. As a result, any measurement of a deuterium abundance establishes an upper bound on which is robust. Thus, the recent measurements of D/H<sup>53</sup> at least

provide a lower bound on  $D/H$ ,  $D/H > 2.1 \times 10^{-5}$  (2) and hence provide an upper bound to  $\Omega_{10} < 7.3$  and  $\Omega_B h^2 < 0.027$ .

Helium-3 can be measured through its hyperfine emission in the radio band, and has been observed in H II regions in our Galaxy. These observations find<sup>58</sup> that there are no obvious trends in  $^3\text{He}$  with metallicity and location in the Galaxy. There is, however, considerable scatter in the data by a factor of 2, some of which may be real. Unfortunately, the stellar and Galactic evolution of  $^3\text{He}$  is not yet sufficiently well understood to constrain whether  $^3\text{He}$  is increasing or decreasing from its primordial value<sup>59</sup>. Consequently, it is unclear whether the observed  $^3\text{He}$  abundance represents an upper or lower limit to the primordial value. Therefore, we can not use  $^3\text{He}$  abundance as a constraint.

By combining the predictions of BBN calculations with the abundances of  $D$ ,  $^4\text{He}$ , and  $^7\text{Li}$  discussed above one can determine the 95% CL region  $4.9 < \Omega_{10} < 6.4$ , with the peak value occurring at  $\Omega_{10} = 5.6$ . This range corresponds to values of  $\Omega_B$  between

$$0.018 < \Omega_B h^2 < 0.023 \quad (24)$$

with a central value of  $\Omega_B h^2 = 0.020$ .

If we were to use only the deuterium abundance from Eq. 23, one obtains the 95% CL range  $5.3 < \Omega_{10} < 7.3$ , with the peak value occurring at  $\Omega_{10} = 5.9$ . This range corresponds to values of  $\Omega_B$  between

$$0.019 < \Omega_B h^2 < 0.027 \quad (25)$$

with a central value of  $\Omega_B h^2 = 0.021$ . As one can see from a comparison with Table 1, these values are in excellent agreement with determinations from the CMB.

## 2.2. Candidates

### 2.2.1. Baryons

Accepting the dark matter hypothesis, the first choice for a candidate should be something we know to exist, baryons. Though baryonic dark matter can not be the whole story if  $\Omega_m > 0.1$ , the identity of the dark matter in galactic halos, which appear to contribute at the level of  $\sim 0.05$ , remains an important question needing to be resolved. A baryon density of this magnitude is not excluded by nucleosynthesis. Indeed we know some of the baryons are dark since  $\Omega_b < 0.01$  in the disk of the galaxy.

It is interesting to note that until recently, there seemed to be some difficulty in reconciling the baryon budget of the Universe. By counting the

visible contribution to  $\tau_{\text{vis}}$  in stellar populations and the X-ray producing hot gas, Persic and Salucci<sup>60</sup> found only  $\tau_{\text{vis}} \approx 0.003$ . A subsequent accounting by Fukugita, Hogan and Peebles<sup>61</sup> found slightly more ( $\approx 0.02$ ) by including the contribution from plasma in groups and clusters. At high redshift on the other hand, all of the baryons can be accounted for. The observed opacity of the Lyman forest in QSO absorption spectra requires a large baryon density consistent with the determinations by the CMB and BBN<sup>62</sup>.

In galactic halos, however, it is quite difficult to hide large amounts of baryonic matter<sup>63</sup>. Sites for halo baryons that have been discussed include hydrogen (frozen, cold or hot gas), low mass stars/Jupiters, remnants of massive stars such as white dwarfs, neutron stars or black holes. In almost every case, a serious theoretical or observational problem is encountered.

#### 2.2.1.1 Hydrogen

A halo predominantly made of hydrogen (with a primordial mixture of  $^4\text{He}$ ) is perhaps the simplest possibility. Hydrogen may however be present in a condensed snowball like state or in the form of gas. Aside from the obvious question of how do these snowballs get made, it is possible to show that their existence today requires them to be so large as to be gravitationally bound<sup>63</sup>.

Assuming that these objects are electrostatically bound, the average density of solid hydrogen is  $\rho_s = 0.07 \text{ g cm}^{-3}$  and the binding energy per molecule is about 1 eV. Given that the average velocity of a snowball is  $v = 250 \text{ km s}^{-1}$ , corresponding to a kinetic energy  $E_k = 600 \text{ eV}$ , snowballs must be collisionless in order to survive. Requiring that the collision rate  $\rho_c = n_s v$  be less than  $t_u^{-1}$  ( $t_u$  is the age of the halo / age of the Universe) with  $n_s = \rho_H m_s$  and  $\rho_H = r_s^{-3}$  one finds  $r_s > 2 \text{ cm}$  and  $m_s > 1 \text{ g}$ , assuming a halo density  $\rho_H = 1.7 \times 10^{-26} \text{ g cm}^{-3}$  (corresponding to  $10^{12} M_\odot$  in a radius of 100 kpc). However, collisionless snowballs also require that their formation occur when the overall density  $\rho = \rho_H$ . In this case, snowballs could not have formed later than a redshift  $(1+z) = 3.5$  or when the microwave background temperature was 9.5K. At this temperature, there is no equilibrium between the gaseous and condensed state and the snowballs would sublimate. For a snowball to survive,  $r_s > 10^{16} \text{ cm}$  is required making this no longer an electrostatically bound object.

If snowballs sublimate, then we can consider the possibility of a halo composed of cold hydrogen gas. Because the collapse time-scale for the halo ( $< 10^9$  yrs) is much less than the age of the galaxy, the gas must be

in hydrostatic equilibrium. Combining the equation of state

$$P(r) = (2\pi m_p) kT \quad (26)$$

where  $m_p$  is the proton mass, with

$$\frac{dP(r)}{dr} = -\frac{GM(r)}{r^2} \quad (27)$$

one can solve for the equilibrium temperature

$$T = \frac{GM(r)}{4kr}, \quad 1.3 \times 10^6 K \quad (28)$$

This is hot gas. As discussed earlier, hot gas is observed through X-ray emission. It is easy to show that an entire halo of hot gas would contract severely with observations. Cooling of course may occur, but at the expense of star formation.

### 2.2.1.2 Jupiter-like objects

A very popular candidate for baryonic dark matter is a very low mass star or JLO. These are objects with a mass  $m < m_{\odot} = 0.08M_{\odot}$ , the mass necessary to commence nuclear burning. Presumably there is a minimum mass<sup>64</sup>  $m > m_{\text{min}} = (0.004 - 0.007)M_{\odot}$  based on fragmentation, but the exact value is very uncertain. The contribution of these objects to the dark matter in the halo depends on how much mass can one put between  $m_{\text{min}}$  and  $m_{\odot}$  and depends on the initial mass function (IMF) in the halo.

An IMF is the number of stars formed per unit volume per unit mass and can be parameterized as

$$= A m^{-(1+x)} \quad (29)$$

In this parameterization, the Salpeter mass function corresponds to  $x = 1.35$ . Because stars are not observed with  $m < m_{\odot}$ , some assumptions about the IMF for low masses must be made. An example of the observed<sup>65</sup> IMF in the solar neighborhood is shown in Fig. 7.

It is possible to use infrared observations<sup>66</sup> to place a lower limit on the slope,  $x$ , of the IMF in the halo of galaxies by comparing a mass-to-light ratio defined by

$$Q = (m = L) L / M \quad (30)$$

where the total mass density in JLO's and low mass stars is given by

$$\frac{Z}{m} = \frac{m}{m_{\text{min}}} dm \quad (31)$$

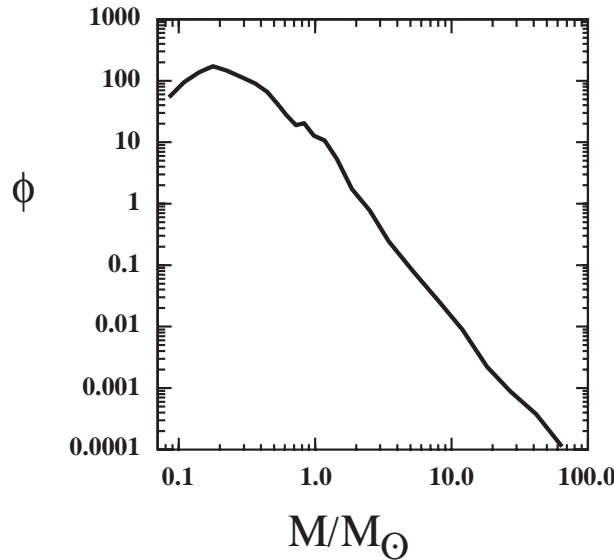


Figure 7. The IM F in the solar neighborhood<sup>65</sup>.

where  $m_g = 0.75M$  is the mass of a giant. The luminosity density given by such a stellar distribution is

$$L = \frac{Z_{m_g}}{m_0} L dm + L_g \quad (32)$$

where  $L(m)$  is the luminosity of a star of mass  $m$ .  $L_g$  is the contribution to the luminosity density due to giant stars. The observed<sup>66</sup> lower limits on  $\phi$  translate to a limit<sup>63</sup> on  $x$

$$x > 1.7 \quad (33)$$

with a weak dependence of  $m_{min}$ .

Unfortunately, one can not use Eq. (33) to exclude JLO's since we do not observe an IM F in the halo and it may be different from that in the disk. One can however make a comparison with existing observations, none of which show such a steep slope at low masses. Indeed, most observations leading to a determination of the IM F (such as the one shown in Fig. 7) show a turnover (or negative slope). To fully answer the questions regarding JLO's in the halo, one needs a better understanding of star formation and the IM F. For now, postulating the existence of a large fraction of JLO's in halo is rather ad-hoc.

Despite the theoretical arguments against them, JLO's own massive compact halo objects (MACHOs) are candidates which are testable by the gravitational microlensing of stars in a neighboring galaxy such as the LMC<sup>67</sup>. By observing millions of stars and examining their intensity as a function of time, it is possible to determine the presence of dark objects in our halo. It is expected that during a lensing event, a star in the LMC will have its intensity rise in an achromatic fashion over a period  $t \propto M^{-3}$  days. Indeed, microlensing candidates have been found<sup>68</sup>. For low mass objects, those with  $M < 0.1M_{\odot}$ , it appears however that the halo fraction of MACHOs is very small. The relative amount of mACHOs in the halo is typically expressed in terms of an optical depth. A halo consisting 100% of mACHOs would have an optical depth of  $5 \times 10^7$ . The most recent results of the MACHO collaboration<sup>69</sup> indicate that  $\tau = 12^{+4}_{-3} \times 10^{-8}$ , corresponding to a mACHO halo fraction of about 20% with a 95% CL range of 8 { 50% based on 13 { 17 events. They also exclude a 100% mACHO halo at the 95% CL. The typical mACHO mass falls in the range  $0.15 \{ 0.9 M_{\odot}$ . The EROS collaboration has set even stronger limits having observed 5 events toward the LMC and 4 toward the SMC<sup>70</sup>. The observed optical depth from EROS1 is  $\tau = 4^{+10}_{-4} \times 10^{-8}$  and from EROS2  $\tau = 6^{+5}_{-3} \times 10^{-8}$ . They have excluded low mass objects ( $M < 0.1M_{\odot}$ ) to make up less than 10% of the halo and objects with  $2 \times 10^7 M_{\odot} < M < 1M_{\odot}$  to be less than 25% of the halo at the 95% CL.

### 2.2.1.3 Remnants of Massive Stars

Next one should possibility that the halo is made up of the dead stellar remnants of stars whose initial masses were  $M > 1M_{\odot}$ . Briefly, the problem which arises in this context is that since at least 40% of the stars initial mass is ejected, and most of this mass is in the form of heavy elements, a large population of these objects would contaminate the disk and prevent the existence of extremely low metallicity objects ( $Z = 10^{-5}$ ) which have been observed. Thus either dust (from ejecta) or dead remnants would be expected to produce too large a metallicity<sup>63,71</sup>. Clearly star formation is a very inefficient mechanism for producing dark matter. Many generations of stars would be required to cycle through their lifetimes to continually trap more matter in remnants.

This question has been studied in more detail<sup>72</sup>. By allowing a variable star formation rate, and allowing a great deal of flexibility in the IMF, a search for a consistent set of parameters so that the halo could be described primarily in terms of dead remnants (in this case white dwarfs) was per-

formed. While a consistent set of chemical evolution parameters can be found, there is no sensible theory to support this choice. In such a model however, the dark matter is in the form of white dwarfs and the remaining gas is heavily contaminated by Carbon and Nitrogen<sup>73</sup>. Though it is not excluded, it is hard to understand this corner of parameter space as being realistic.

#### 2.2.1.4 Black Holes

There are several possibilities for black holes as the dark matter in halos. If the black holes are primordial<sup>74</sup> which have presumably formed before nucleosynthesis, they should not be counted as baryonic dark matter and therefore do not enter into the present discussion. If the black holes are formed as the final stage of star's history and its formation was preceded by mass loss or a supernovae, then the previous discussion on remnants of massive stars applies here as well. However, it is also possible that the black halos were formed directly from very massive stars ( $m > 100M_{\odot}$ ?) through gravitational instability with no mass loss<sup>75</sup>. Though there are limits due to overheating the disk<sup>76</sup> and stellar systems<sup>77</sup>. In this case I know of no argument preventing a sufficiently large population of massive black holes as baryonic dark matter (Of course, now the IMF must have  $m_{min} > 100M_{\odot}$  :)

#### 2.2.2. Neutrinos

Light neutrinos ( $m \sim 30\text{eV}$ ) are a long-time standard when it comes to non-baryonic dark matter<sup>78</sup>. Light neutrinos produce structure on large scales, and the natural (minimal) scale for structure clustering is given in Eq. (15). Hence neutrinos offer the natural possibility for large scale structures<sup>79,80</sup> including filaments and voids. Light neutrinos are, however, ruled out as a dominant form of dark matter because they produce too much large scale structure<sup>81</sup>. Because the smallest non-linear structures have mass scale  $M_J$  and the typical galactic mass scale is  $\sim 10^{12}M_{\odot}$ , galaxies must fragment out of the larger pancake-like objects. The problem with such a scenario is that galaxies form late<sup>80,82</sup> ( $z > 1$ ) whereas quasars and galaxies are seen out to redshifts  $z > 6$ .

In the standard model, the absence of a right-handed neutrino state precludes the existence of a neutrino mass (unless one includes non-renormalizable lepton number violating interactions such as HLL). By adding a right-handed state  $\nu_R$ , it is possible to generate a Dirac mass for

the neutrino,  $m = h v = \frac{p}{2}$ , as is the case for the charged lepton masses, where  $h$  is the neutrino Yukawa coupling constant, and  $v$  is the Higgs expectation value. It is also possible to generate a Majorana mass for the neutrino when in addition to the Dirac mass term,  $m_{RL}$ , a term  $M_{RR}$  is included. If  $M > m$ , the see-saw mechanism produces two mass eigenstates given by  $m_1 < M$  which is very light, and  $m_2 > M$  which is heavy. The state  $_1$  is a potential hot dark matter candidate as  $_2$  is in general not stable.

The simplicity of the standard big bang model allows one to compute in a straightforward manner the relic density of any stable particle if that particle was once in thermal equilibrium with the thermal radiation bath. At early times, neutrinos were kept in thermal equilibrium by their weak interactions with electrons and positrons. As we saw in the case of the  $\gamma$ -interaction used in BBN, one can estimate the thermally averaged low-energy weak interaction scattering cross section

$$h v i \cdot g^4 T^2 = m_W^4 \quad (34)$$

for  $T \ll m_W$ . Recalling that the number density scales as  $n \propto T^3$ , we can compare the weak interaction rate  $nh vi$ , with the expansion rate given by eqs. (6) with

$$= \frac{X_B}{g_B} + \frac{7X_F}{8g_F} \frac{1}{30} T^4 - \frac{2}{30} N(T) T^4 \quad (35)$$

Neutrinos will be in equilibrium when  $w_k > H$  or

$$T^3 > \frac{P}{8^3 N} = 90 \cdot m_W^4 = M_P \quad (36)$$

where  $M_P = G_N^{1/2} = 1.22 \cdot 10^9$  GeV is the Planck mass. For  $N = 43 = 4$  (accounting for photons, electrons, positrons and three neutrino flavors) we see that equilibrium is maintained at temperatures greater than  $0(1)$  MeV (for a more accurate calculation see <sup>83</sup>).

The decoupling scale of  $0(1)$  MeV has an important consequence on the initial relic density of massive neutrinos. Neutrinos more massive than 1 MeV will begin to annihilate prior to decoupling, and while in equilibrium, their number density will become exponentially suppressed. Lighter neutrinos decouple as radiation on the other hand, and hence do not experience the suppression due to annihilation. Therefore, the calculations of the number density of light ( $m < 1$  MeV) and heavy ( $m > 1$  MeV) neutrinos differ substantially.

The number of density of light neutrinos with  $m < 1 \text{ MeV}$  can be expressed at late times as

$$= m Y n \quad (37)$$

where  $Y = n = n$  is the density of 's relative to the density of photons, which today is 411 photons per  $\text{cm}^3$ . It is easy to show that in an adiabatically expanding universe  $Y = 3=11$ . This suppression is a result of the  $e^+ e^-$  annihilation which occurs after neutrino decoupling and heats the photon bath relative to the neutrinos. In order to obtain an age of the Universe,  $t > 12 \text{ G yr}$ , one requires that the matter component is constrained by

$$h^2 < 0.3: \quad (38)$$

From this one finds the strong constraint (upper bound) on the matter neutrino masses<sup>84</sup>:

$$m_{\text{tot}} = \sum^X m < 28 \text{ eV} : \quad (39)$$

where the sum runs over neutrino mass eigenstates. The limit for Dirac neutrinos depends on the interactions of the right-handed states (see discussion below). Given the discussion of the CMB results in the previous section, one could make a case that the limit on  $h^2$  should be reduced by a factor of 2, which would translate into a limit of 14 eV on the sum of the light neutrino masses. As one can see, even very small neutrino masses of order 1 eV, may contribute substantially to the overall relic density. The limit (39) and the corresponding initial rise in  $h^2$  as a function of  $m$  is displayed in the Figure 8 (the low mass end with  $m < 1 \text{ MeV}$ ).

Combining the rapidly improving data on key cosmological parameters with the better statistics from large redshift surveys has made it possible to go a step forward along this path. It is now possible to set stringent limits on the light neutrino mass density  $h^2$ , and hence on the neutrino mass based on the power spectrum of the Lyman forest<sup>86</sup>,  $m_{\text{tot}} < 5.5 \text{ eV}$ , and the limit is even stronger if the total matter density,  $m$ , is less than 0.5. Adding additional observation constraints from the CMB and galaxy clusters drops this limit<sup>87</sup> to 2.4 eV. This limit has recently been improved by the 2dF Galaxy redshift<sup>88</sup> survey by comparing the derived power spectrum of fluctuations with structure formation models. Focussing on the the presently favoured CDM model, the neutrino mass bound becomes  $m_{\text{tot}} < 1.8 \text{ eV}$  for  $m < 0.5$ . When even more constraints such as HST

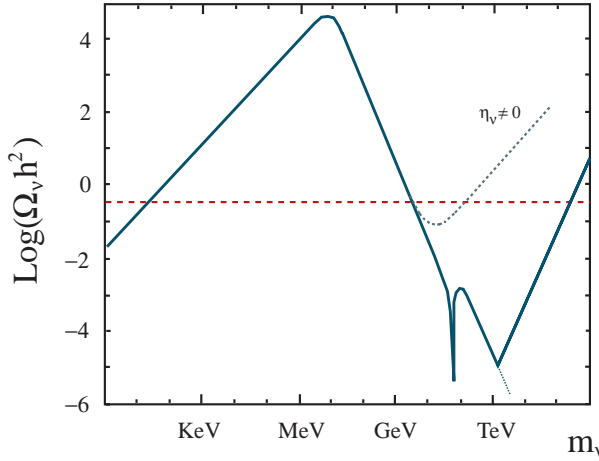


Figure 8. Summary plot<sup>85</sup> of the relic density of Dirac neutrinos (solid) including a possible neutrino asymmetry of  $\eta_\nu = 5 \times 10^{11}$  (dotted).

Key project data, supernovae type Ia data, and BBN are included<sup>89</sup> the limit it can be pushed to  $m_{\text{tot}} < 0.3$  eV.

The calculation of the relic density for neutrinos more massive than 1 MeV, is substantially more involved. The relic density is now determined by the freeze-out of neutrino annihilations which occur at  $T < m$ , after annihilations have begun to seriously reduce their number density<sup>90</sup>. The annihilation rate is given by

$$\text{ann} = h v i_{\text{ann}} n \frac{m^2}{m^4_Z} (n - T)^{3=2} e^{m - T} \quad (40)$$

where we have assumed, for example, that the annihilation cross section is dominated by  $1/4\pi v^2$  via Z-boson exchange<sup>a</sup> and  $h v i_{\text{ann}} = m^2 = m_Z^4$ . When the annihilation rate becomes slower than the expansion rate of the Universe the annihilations freeze out and the relative abundance of neutrinos becomes fixed. For particles which annihilate through approximate weak scale interactions, this occurs when  $T = m = 20$ . The number density

<sup>a</sup>While this is approximately true for Dirac neutrinos, the annihilation cross section of Majorana neutrinos is p-wave suppressed and is proportional of the final state fermion masses rather than  $m$ .

of neutrinos is tracked by a Boltzmann-like equation,

$$\frac{dn}{dt} = \frac{R}{R} n h v_i (f^2 - f_0^2) \quad (41)$$

where  $n_0$  is the equilibrium number density of neutralinos. By defining the quantity  $f = n/T^3$ , we can rewrite this equation in terms of  $x$ , as

$$\frac{df}{dx} = m \frac{8}{90} G_N N^{1/2} (f^2 - f_0^2) \quad (42)$$

The solution to this equation at late times (small  $x$ ) yields a constant value of  $f$ , so that  $n \propto T^3$ .

Roughly, the solution to the Boltzmann equation goes as  $f \propto (m h v_{i\text{ann}})^{-1}$  and hence  $h^2 \propto h v_{i\text{ann}}^{-1}$ , so that parametrically  $h^2 \propto 1/m^2$ . As a result, the constraint (38) now leads to a lower bound<sup>90,91,92</sup> on the neutrino mass, of about  $m > 3-7$  GeV, depending on whether it is a Dirac or Majorana neutrino. This bound and the corresponding downward trend  $h^2 \propto 1/m^2$  can again be seen in Figure 8. The result of a more detailed calculation is shown in Figure 9<sup>92</sup> for the case of a Dirac neutrino. The two curves show the slight sensitivity on the temperature scale associated with the quark-hadron transition. The result for a Majorana mass neutrino is qualitatively similar. Indeed, any particle with roughly weak scale cross-sections will tend to give an interesting value of  $h^2 \approx 1$ .

The deep drop in  $h^2$ , visible in Figure 8 at around  $m = M_Z = 2$ , is due to a very strong annihilation cross section at  $Z$ -boson pole. For yet higher neutrino masses the  $Z$ -annihilation channel cross section drops as  $1/m^2$ , leading to a brief period of an increasing trend in  $h^2$ . However, for  $m > m_W$  the cross section regains its parametric form  $h v_{i\text{ann}} \propto m^2$  due to the opening up of a new annihilation channel to  $W$ -boson pairs<sup>93</sup>, and the density drops again as  $h^2 \propto 1/m^2$ . The tree level  $W$ -channel cross section breaks the unitarity at around 0 (few) TeV<sup>94</sup> however, and the full cross section must be bound by the unitarity limit<sup>95</sup>. This behaves again as  $1/m^2$ , whereby  $h^2$  has to start increasing again, until it becomes too large again at 200-400 TeV<sup>95,94</sup> (or perhaps somewhat earlier as the weak interactions become strong at the unitarity breaking scale).

If neutrinos are Dirac particles, and have a nonzero asymmetry the relic density could be governed by the asymmetry rather than by the annihilation cross section. Indeed, it is easy to see that the neutrino mass density corresponding to the asymmetry  $(n_+ - n_-)/n$  is given by<sup>96</sup>

$$= m \quad n ; \quad (43)$$

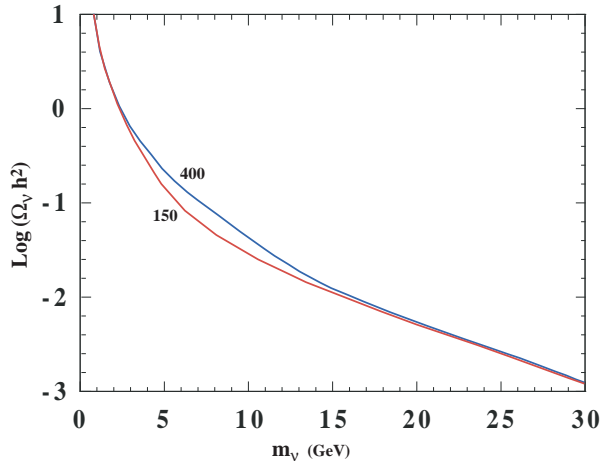


Figure 9. The relic density of heavy Dirac neutrinos due to annihilations<sup>92</sup>. The curves are labeled by the assumed quark-hadron phase transition temperature in MeV.

which implies

$$h^2 \leq 0.004 \quad (m = \text{GeV}): \quad (44)$$

where  $m_{10} = 10^{10}$ . The behaviour of the energy density of neutrinos with an asymmetry is shown by the dotted line in the Figure 8. At low  $m$ , the mass density is dominated by the symmetric, relic abundance of both neutrinos and antineutrinos which have already frozen out. At higher values of  $m$ , the annihilations suppress the symmetric part of the relic density until  $h^2$  eventually becomes dominated by the linearly increasing asymmetric contribution. In the figure, we have assumed an asymmetry of  $5 \times 10^{-11}$  for neutrinos with standard weak interaction strength. In this case,  $h^2$  begins to rise when  $m > 20$  GeV. Obviously, the bound (38) is saturated for  $m = 75$  GeV =  $m_{10}$ .

Based on the leptonic and invisible width of the Z boson, experiments at LEP have determined that the number of neutrinos is  $N = 2.9841 \pm 0.0083$ <sup>97</sup>. Conversely, any new physics must fit within these brackets, and thus LEP excludes additional neutrinos (with standard weak interactions) with masses  $m < 45$  GeV. Combined with the limits displayed in Figures 8 and 9, we see that the mass density of ordinary heavy neutrinos is bound to be very small,  $h^2 < 0.001$  for masses  $m > 45$  GeV up to  $m = 0$  (100) TeV. Lab constraints for Dirac neutrinos are

available<sup>98</sup>, excluding neutrinos with masses between 10 GeV and 4.7 TeV. This is significant, since it precludes the possibility of neutrino dark matter based on an asymmetry between  $\nu_e$  and  $\nu_{\mu}$ . Majorana neutrinos are excluded as dark matter since  $h_o^2 < 0.001$  for  $m > 45$  GeV and are thus cosmologically uninteresting.

A bound on neutrino masses even stronger than Eqn. (39) can be obtained from the recent observations of active-active mixing in both solar- and atmospheric neutrino experiments. The inferred evidence for  $\nu_e$  and  $\nu_{\mu}$ , mixings are on the scales  $m^2 = 1 \text{ to } 10^5$  and  $m^2 = 2 \text{ to } 5 \times 10^3$ . When combined with the upper bound on the electron-like neutrino mass  $m < 2.8$  eV<sup>99</sup>, and the LEP limits on the number of neutrino species, one finds the constraint on the sum of neutrino masses:

$$0.05 \text{ eV} < m_{\text{tot}} < 8.4 \text{ eV} : \quad (45)$$

Conversely, the experimental and observational data then implies that the cosmological energy density of all light, weakly interacting neutrinos can be restricted to the range

$$0.0005 < h^2 < 0.09 : \quad (46)$$

Interestingly there is now also a lower bound due to the fact that at least one of the neutrino masses has to be larger than the scale  $m^2 = 10^3 \text{ eV}^2$  set by the atmospheric neutrino data. Combined with the results on relic mass density of neutrinos and the LEP limits, the bound (46) implies that the ordinary weakly interacting neutrinos, once the standard dark matter candidate<sup>78</sup>, can be ruled out completely as a dominant component of the dark matter.

If instead, we consider right-handed neutrinos, we have new possibilities. Right-handed interactions are necessarily weaker than standard left-handed interactions implying that right-handed neutrinos decouple early and today are at a reduced temperature relative to  $T_L = 100$

$$\left(\frac{T_R}{T_L}\right)^3 = \frac{43}{4N(T_d)} \quad (47)$$

As such, for  $T_{dR} = 1$  MeV,  $n_R = n_L = (T_R = T_L)^3 = 1$ . Thus the abundance of right-handed neutrinos can be written as

$$Y_R = \frac{n_R}{n} = \left(\frac{3}{11}\right) \left(\frac{T_R}{T_L}\right)^3 = \frac{3}{11} \quad (48)$$

In this case, the previous bound (39) on neutrino masses is weakened. For a suitably large scale for the right-handed interactions, right-handed neutrino

masses may be as large as a few keV<sup>101</sup>. Such neutrinos make excellent warm dark matter candidates, albeit the viable mass range for galaxy formation is quite restricted<sup>102</sup>.

### 2.2.3. Axions

Due to space limitations, the discussion of this candidate will be very brief. Axions are pseudo-Goldstone bosons which arise in solving the strong CP problem<sup>103,104</sup> via a global U(1) Peccei-Quinn symmetry. The invisible axion<sup>104</sup> is associated with the direction of the spontaneously broken PQ symmetry. Because the PQ symmetry is also explicitly broken (the CP violating  $F\bar{F}$  coupling is not PQ invariant) the axion picks up a small mass similar to pion picking up a mass when chiral symmetry is broken. We can expect that  $m_a \sim f_a$  where  $f_a$ , the axion decay constant, is the vacuum expectation value of the PQ current and can be taken to be quite large. If we write the axion field as  $a = f_a \phi$ , near the minimum, the potential produced by QCD instanton effects looks like  $V \sim m_a^2 \phi^2 f_a^2$ . The axion equations of motion lead to a relatively stable oscillating solution. The energy density stored in the oscillations exceeds the critical density<sup>105</sup> unless  $f_a < 10^{12}$  GeV.

Axions may also be emitted stars and supernovae<sup>106</sup>. In supernovae, axions are produced via nucleon-nucleon bremsstrahlung with a coupling  $g_{AN} / m_N = f_a$ . As was noted above the cosmological density limit requires  $f_a < 10^{12}$  GeV. Axion emission from red giants imply<sup>107</sup>  $f_a > 10^{10}$  GeV (though this limit depends on an adjustable axion-electron coupling), the supernova limit requires<sup>108</sup>  $f_a > 2 \times 10^{11}$  GeV for naive quark model couplings of the axion to nucleons. Thus only a narrow window exists for the axion as a viable dark matter candidate.

## 3. Lecture 3: Supersymmetric Dark Matter

Although there are many reasons for considering supersymmetry as a candidate extension to the standard model of strong, weak and electromagnetic interactions<sup>109</sup>, one of the most compelling is its role in understanding the hierarchy problem<sup>110</sup> namely, why/how is  $m_W \ll M_P$ . One might think naively that it would be sufficient to set  $m_W \ll M_P$  by hand. However, radiative corrections tend to destroy this hierarchy. For example, one-loop diagrams generate

$$m_W^2 = 0 - \frac{1}{2} m_W^2 \quad (49)$$

where  $\epsilon$  is a cut-off representing the appearance of new physics, and the inequality in (49) applies if  $m \gtrsim 10^3$  TeV, and even more so if  $m_{GUT} \gtrsim 10^{16}$  GeV or  $M_p \gtrsim 10^9$  GeV. If the radiative corrections to a physical quantity are much larger than its measured values, obtaining the latter requires strong cancellations, which in general require fine tuning of the bare input parameters. However, the necessary cancellations are natural in supersymmetry, where one has equal numbers of bosons and fermions with equal couplings, so that (49) is replaced by

$$m_W^2 = 0 - j n_B^2 - m_F^2 j : \quad (50)$$

The residual radiative correction is naturally small if  $j n_B^2 - m_F^2 j \ll 1$  TeV<sup>2</sup>.

In order to justify the absence of interactions which can be responsible for extremely rapid proton decay, it is common in the minimal supersymmetric standard model (MSSM) to assume the conservation of R-parity. If R-parity, which distinguishes between "normal matter" and the supersymmetric partners and can be defined in terms of baryon, lepton and spin as  $R = (-1)^{3B+L+2S}$ , is unbroken, there is at least one supersymmetric particle (the lightest supersymmetric particle or LSP) which must be stable. Thus, the minimal model contains the fewest number of new particles and interactions necessary to make a consistent theory.

There are very strong constraints, however, forbidding the existence of stable or long lived particles which are not color and electrically neutral<sup>111</sup>. Strong and electromagnetically interacting LSPs would become bound with normal matter forming anomalously heavy isotopes. Indeed, there are very strong upper limits on the abundances, relative to hydrogen, of nuclear isotopes<sup>112</sup>,  $n = n_H \ll 10^{-15}$  to  $10^{-29}$  for  $1 \text{ GeV} \leq m \leq 1 \text{ TeV}$ . A strongly interacting stable relic is expected to have an abundance  $n = n_H \ll 10^{-10}$  with a higher abundance for charged particles.

There are relatively few supersymmetric candidates which are not colored and are electrically neutral. The sneutrino<sup>113</sup> is one possibility, but in the MSSM, it has been excluded as a dark matter candidate by direct<sup>98</sup> and indirect<sup>114</sup> searches. In fact, one can set an accelerator based limit on the sneutrino mass from neutrino counting,  $m \sim 44.7 \text{ GeV}$ <sup>115</sup>. In this case, the direct relic searches in underground low-background experiments require  $m \sim 20 \text{ TeV}$ <sup>98</sup>. Another possibility is the gravitino which is probably the most difficult to exclude. I will concentrate on the remaining possibility in the MSSM, namely the neutralinos.

### 3.1. Parameters

The most general version of the MSSM, despite its minimality in particles and interactions contains well over a hundred new parameters. The study of such a model would be untenable were it not for some (well-motivated) assumptions. These have to do with the parameters associated with supersymmetry breaking. It is often assumed that, at some unification scale, all of the gaugino masses receive a common mass,  $m_{1=2}$ . The gaugino masses at the weak scale are determined by running a set of renormalization group equations. Similarly, one often assumes that all scalars receive a common mass,  $m_0$ , at the GUT scale. These too are run down to the weak scale. The remaining parameters of importance involve the Higgs sector. There is the Higgs mixing mass parameter,  $\lambda$ , and since there are two Higgs doublets in the MSSM, there are two vacuum expectation values. One combination of these is related to the  $Z$  mass, and therefore is not a free parameter, while the other combination, the ratio of the two vevs,  $\tan\beta$ , is free.

If the supersymmetry breaking Higgs soft masses are also unified at the GUT scale (and take the common value  $m_0$ ), then and the physical Higgs masses at the weak scale are determined by electroweak vacuum conditions ( $\lambda$  is determined up to a sign). This scenario is often referred to as the constrained MSSM or CMSSM. Once these parameters are set, the entire spectrum of sparticle masses at the weak scale can be calculated<sup>b</sup>. In Fig. 10, an example of the running of the mass parameters in the CMSSM is shown. Here, we have chosen  $m_{1=2} = 250$  GeV,  $m_0 = 100$  GeV,  $\tan\beta = 3$ ,  $A_0 = 0$ , and  $\lambda < 0$ . Indeed, it is rather amazing that from so few input parameters, all of the masses of the supersymmetric particles can be determined. The characteristic features that one sees in the figure, are for example, that the colored sparticles are typically the heaviest in the spectrum. This is due to the large positive correction to the masses due to  $\lambda$  in the RGE's. Also, one finds that the  $B^0$  (the partner of the  $U(1)_Y$  gauge boson), is typically the lightest sparticle. But most importantly, notice that one of the Higgs masses<sup>2</sup>, goes negative triggering electroweak symmetry breaking<sup>116</sup>. (The negative sign in the figure refers to the sign of the mass<sup>2</sup>, even though it is the mass of the sparticles which are depicted.)

---

<sup>b</sup> There are in fact, additional parameters: the supersymmetry-breaking trilinear masses  $A$  (also assumed to be unified at the GUT scale) as well as two CP violating phases and  $A$ .

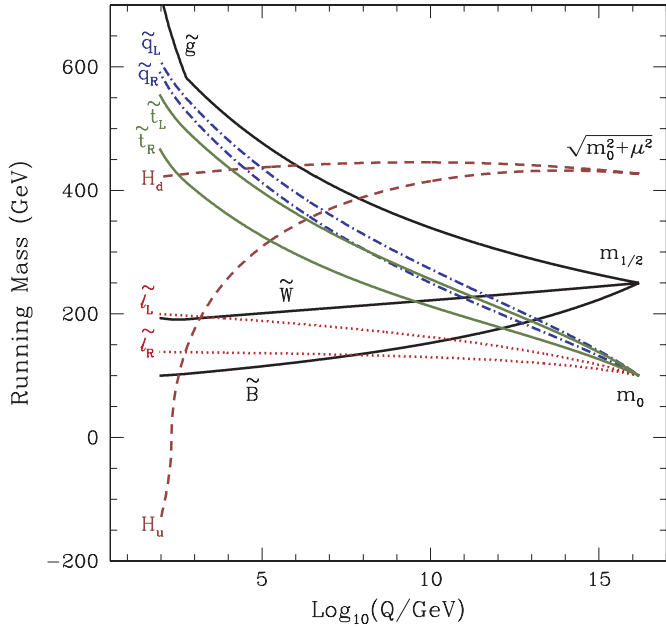


Figure 10. RG evolution of the mass parameters in the CM SSM.

### 3.2. Neutralinos

There are four neutralinos, each of which is a linear combination of the  $R = 1$  neutral fermions<sup>111</sup>: the wino  $W^3$ , the partner of the 3rd component of the  $SU(2)_L$  gauge boson; the bino,  $B^0$ ; and the two neutral Higgsinos,  $H_1^0$  and  $H_2^0$ . Assuming gaugino mass universality at the GUT scale, the identity and mass of the LSP are determined by the gaugino mass  $m_{1/2}$ , and  $\tan\beta$ . In general, neutralinos can be expressed as a linear combination

$$= \mathbf{B} + \mathbf{W}^3 + \mathbf{H}_1 + \mathbf{H}_2 \quad (51)$$

The solution for the coe cients ; ; and for neutralinos that m ake up the LSP can be found by diagonalizing the m ass m atrix

$$\begin{array}{ccccccccc}
 & 0 & & M_2 & & 0 & & \frac{g_3 v_1}{2} & & 1 & 0 & W^3 & 1 \\
 & \frac{g_2 v_1}{2} & & 0 & & M_1 & & \frac{g_1 v_1}{2} & & \frac{g_1 v_2}{2} & C & \frac{g_1 v_1}{2} & C \\
 (W^3; B; H_1^0; H_2^0) @& \frac{g_2 v_1}{2} & & \frac{g_1 v_1}{2} & & 0 & & 0 & & \frac{g_1 v_2}{2} & C & \frac{g_1 v_1}{2} & C \\
 & \frac{g_3 v_2}{2} & & \frac{g_1 v_2}{2} & & & & & & & A & H_1^0 & A \\
 & \frac{g_3 v_2}{2} & & \frac{g_1 v_2}{2} & & & & & & & H_2^0 & & 
 \end{array} \quad (52)$$

where  $M_1$  ( $M_2$ ) is a soft supersymmetry breaking term giving mass to the  $U(1)$  ( $SU(2)$ ) gaugino(s). In a unified theory  $M_1 = M_2 = m_{1=2}$  at the unification scale (at the weak scale,  $M_1 = \frac{5}{3}M_2$ ). As one can see, the coefficients  $\alpha_1, \alpha_2, \alpha_3$  and  $\alpha_4$  depend only on  $m_{1=2}$ ,  $\tan\beta$ , and  $\tan\alpha$ .

In Figure 11<sup>117</sup>, regions in the  $M_2$ ;  $\tan\beta$  plane with  $\tan\alpha = 2$  are shown in which the LSP is one of several nearly pure states, the photino,  $\tilde{\chi}_1^0$ , the bino,  $\tilde{B}$ , a symmetric combination of the Higgsinos,  $\tilde{H}_{12}$ , or the Higgsino,  $\tilde{S} = \sin\tilde{H}_1 + \cos\tilde{H}_2$ . The dashed lines show the LSP mass contours. The crosshatched regions correspond to parameters giving a chargino ( $\tilde{W}^\pm$ ;  $\tilde{H}^\pm$ ) state with mass  $m \sim 45$  GeV and as such are excluded by LEP<sup>118</sup>. This constraint has been extended by LEP<sup>119</sup> and is shown by the light shaded region and corresponds to regions where the chargino mass is  $< 103.5$  GeV. The newer limit does not extend deep into the Higgsino region because of the degeneracy between the chargino and neutralino. Notice that the parameter space is dominated by the  $\tilde{B}$  or  $\tilde{H}_{12}$  pure states and that the photino only occupies a small fraction of the parameter space, as does the Higgsino combination  $\tilde{S}$ . Both of these light states are experimentally excluded.

### 3.3. The Relic Density

The relic abundance of LSP's is determined by solving the Boltzmann equation for the LSP number density in an expanding Universe. The technique<sup>92</sup> used is similar to that for computing the relic abundance of massive neutrinos<sup>90</sup>. The relic density depends on additional parameters in the MSSM beyond  $m_{1=2}$ ,  $\tan\beta$ , and  $\tan\alpha$ . These include the sfermion masses,  $m_f$  and the Higgs pseudo-scalar mass,  $m_A$ , derived from  $m_0$  (and  $m_{1=2}$ ). To determine the relic density it is necessary to obtain the general annihilation cross-section for neutralinos. In much of the parameter space of interest, the LSP is a bino and the annihilation proceeds mainly through sfermion exchange. Because of the p-wave suppression associated with Majorana fermions, the s-wave part of the annihilation cross-section is suppressed by the outgoing fermion masses. This means that it is necessary to expand the cross-section to include p-wave corrections which can be expressed as a term proportional to the temperature if neutralinos are in equilibrium. Unless the neutralino mass happens to lie near near a pole, such as  $m_{\tilde{h}} = m_{\tilde{Z}} = 2$  or  $m_{\tilde{h}} = 2$ , in which case there are large contributions to the annihilation through direct s-channel resonance exchange, the dominant contribution to the  $\tilde{B}\tilde{B}$  annihilation cross section comes from crossed t-channel sfermion

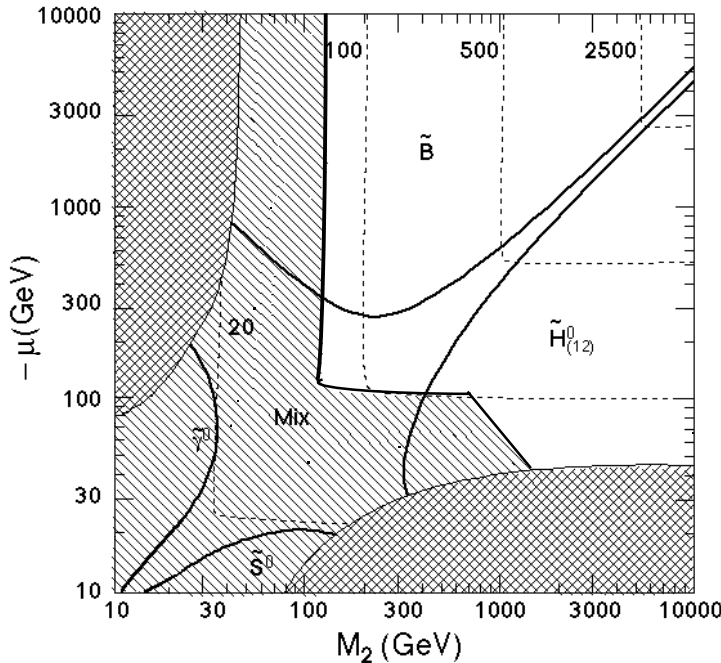


Figure 11. Mass contours and composition of nearly pure LSP states in the M SSM <sup>117</sup>.

exchange.

Annihilations in the early Universe continue until the annihilation rate  $\langle \sigma v \rangle$  drops below the expansion rate. The calculation of the neutralino relic density proceeds in much the same way as discussed above for neutrinos with the appropriate substitution of the cross section. The final neutralino relic density expressed as a fraction of the critical energy density can be written as<sup>111</sup>

$$h^2 \sim 1.9 \cdot 10^{11} \cdot \frac{T}{T_f}^3 \cdot N_f^{1/2} \cdot \frac{GeV}{ax_f + \frac{1}{2}bx_f^2} \quad (53)$$

where  $(T = T_f)^3$  accounts for the subsequent reheating of the photon temperature with respect to  $T_f$ , due to the annihilations of particles with mass  $m < x_f m = 100$ . The subscript  $f$  refers to values at freeze-out, i.e., when annihilations cease. The coefficients  $a$  and  $b$  are related to the partial wave expansion of the cross-section,  $\sigma = a + bx + \dots$ . Eq. (53) results in a very good approximation to the relic density except near s-channel annihilation

poles, thresholds and in regions where the LSP is nearly degenerate with the next lightest supersymmetric particle<sup>120</sup>.

When there are several particle species  $i$ , which are nearly degenerate in mass, co-annihilations are important. In this case<sup>120</sup>, the rate equation (41) still applies, provided  $n$  is interpreted as the total number density,

$$n = \sum_i n_i; \quad (54)$$

$n_0$  as the total equilibrium number density,

$$n_0 = \sum_i n_{0;i}; \quad (55)$$

and the effective annihilation cross section as

$$\langle h_e v_{\text{rel}} \rangle = \sum_{ij} \frac{n_{0;i} n_{0;j}}{n_0^2} h_{ij} v_{\text{rel}}; \quad (56)$$

In eq. (42),  $m$  is now understood to be the mass of the lightest sparticle under consideration.

Note that this implies that the ratio of relic densities computed with and without coannihilations is, roughly,

$$R = \frac{x_e^0}{x_0^0} \frac{x_f^0}{x_f^0}; \quad (57)$$

where  $\hat{x} = a + bx = 2$  and sub- and superscripts 0 denote quantities computed ignoring coannihilations. The ratio  $x_f^0 = x_f \cdot 1 + x_f^0 \ln(g_e - g_{10})$ , where  $g_e = \prod_i g_i (m_i - m_1)^{3/2} e^{-\ln(m_i/m_1) = T}$ . For the case of three degenerate slepton NLSPs<sup>121</sup>,  $g_e = \prod_i g_i = 8$  and  $x_f^0 = x_f \cdot 12$ . The effects of co-annihilations are discussed below.

### 3.4. Phenomenological and Cosmological Constraints

For the cosmological limits on the relic density I will assume

$$0.1 \quad h^2 \quad 0.3; \quad (58)$$

The upper limit being a conservative bound based only on the lower limit to the age of the Universe of 12 G yr. Indeed, most analyses indicate that  $m_{\text{matter}} < 0.4 - 0.5$  and thus it is very likely that  $h^2 < 0.2$  (cf. the CMB results in Table 1). One should note that smaller values of  $h^2$  are allowed, since it is quite possible that some of the cold dark matter might not consist of LSPs.

The calculated relic density is found to have a relevant cosmological density over a wide range of susy parameters. For all values of  $\tan\beta$ , there is a 'bulk' region with relatively low values of  $m_{1=2}$  and  $m_0$  where  $0.1 < h^2 < 0.3$ . However there are a number of regions at large values of  $m_{1=2}$  and/or  $m_0$  where the relic density is still compatible with the cosmological constraints. At large values of  $m_{1=2}$ , the lighter stau becomes nearly degenerate with the neutralino and co-annihilations between these particles must be taken into account<sup>121,122</sup>. For non-zero values of  $A_0$ , there are new regions for which coannihilations are important<sup>123</sup>. At large  $\tan\beta$ , as one increases  $m_{1=2}$ , the pseudo-scalar mass,  $m_A$  begins to drop so that there is a wide funnel-like region (at all values of  $m_0$ ) such that  $2m_A < m_{1=2}$  and s-channel annihilations become important<sup>124,125</sup>. Finally, there is a region at very high  $m_0$  where the value of  $\tan\beta$  begins to fall and the LSP becomes more Higgsino-like. This is known as the 'focus point' region<sup>126</sup>.

As an aid to the assessment of the prospects for detecting sparticles at different accelerators, benchmark sets of supersymmetric parameters have often been found useful, since they provide a focus for concentrated discussion. A set of proposed post-LEP benchmark scenarios<sup>127</sup> in the CM SSM are illustrated schematically in Fig. 12. Five of the chosen points are in the 'bulk' region at small  $m_{1=2}$  and  $m_0$ , four are spread along the co-annihilation 'tail' at larger  $m_{1=2}$  for various values of  $\tan\beta$ . This tail runs along the shaded region in the lower right corner where the stau is the LSP and is therefore excluded by the constraints against charged dark matter. Two points are in rapid-annihilation 'funnels' at large  $m_{1=2}$  and  $m_0$ . At large values of  $m_0$ , the focus-point region runs along the boundary where electroweak symmetry no longer occurs (shown in Fig. 12 as the shaded region in the upper left corner). Two points were chosen in the focus-point region at large  $m_0$ . The proposed points range over the allowed values of  $\tan\beta$  between 5 and 50. The light shaded region corresponds to the portion of parameter space where the relic density  $h^2$  is between 0.1 and 0.3.

The effect of coannihilations is to create an allowed band about 25–50 GeV wide in  $m_0$  for  $m_{1=2} < 1400$  GeV, which tracks above the  $m_e = m_{1=2}$  contour. Along the line  $m_e = m_{1=2}$ , from 57) <sup>121</sup>. As  $m_0$  increases, the mass difference increases and the slepton contribution to  $\hat{m}_e$  falls, and the relic density rises abruptly. This effect is seen in Fig. 13. The light shaded region corresponds to  $0.1 < h^2 < 0.3$ . The dark shaded region has  $m_e < m_{1=2}$  and is excluded. The light dashed contours indicate the corresponding region in  $h^2$  if one ignores the effect of coannihilations.

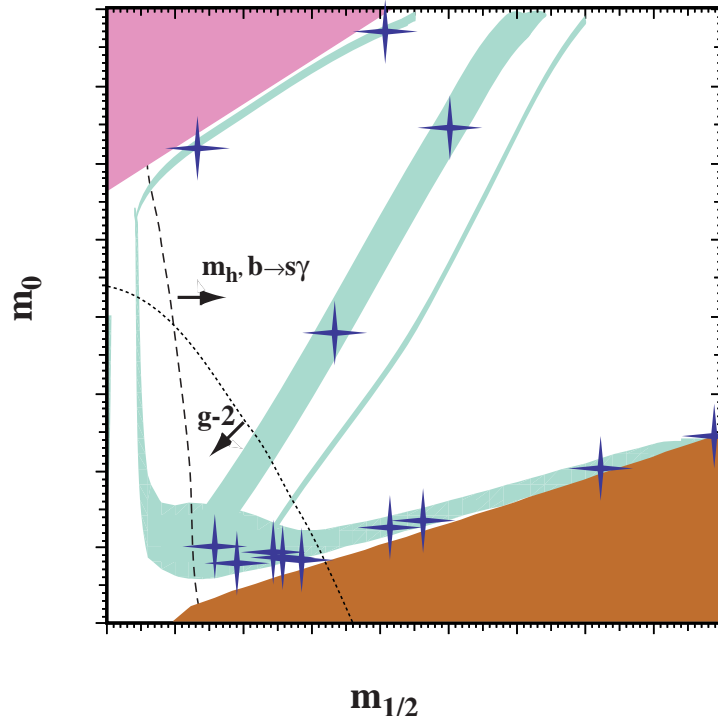


Figure 12. Schematic overview of the CM SSM benchmark points proposed in 127. The points are intended to illustrate the range of available possibilities. The labels correspond to the approximate positions of the benchmark points in the  $(m_{1/2}; m_0)$  plane. They also span values of  $\tan\beta$  from 5 to 50 and include points with  $\tan\beta < 0$ .

Neglecting coannihilations, one would find an upper bound of 450 GeV on  $m_{1/2}$ , corresponding to an upper bound of roughly 200 GeV on  $m_B$ . Instead, values of  $m_{1/2}$  up to 1400 GeV are allowed corresponding to an upper bound of 600 GeV on  $m_B$ .

The most important phenomenological constraints are also shown schematically in Figure 12. These include the constraint provided by the LEP lower limit on the Higgs mass:  $m_h > 114.4$  GeV 128. This holds in the Standard Model, for the lightest Higgs boson  $h$  in the general MSSM for  $\tan\beta < 8$ , and almost always in the CM SSM for all  $\tan\beta$ . Since  $m_h$  is sensitive to sparticle masses, particularly  $m_{\tilde{t}}$ , via loop corrections, the Higgs limit also imposes important constraints on the CM SSM parameters, principally  $m_{1/2}$  as seen by the dashed curve in Fig. 12.

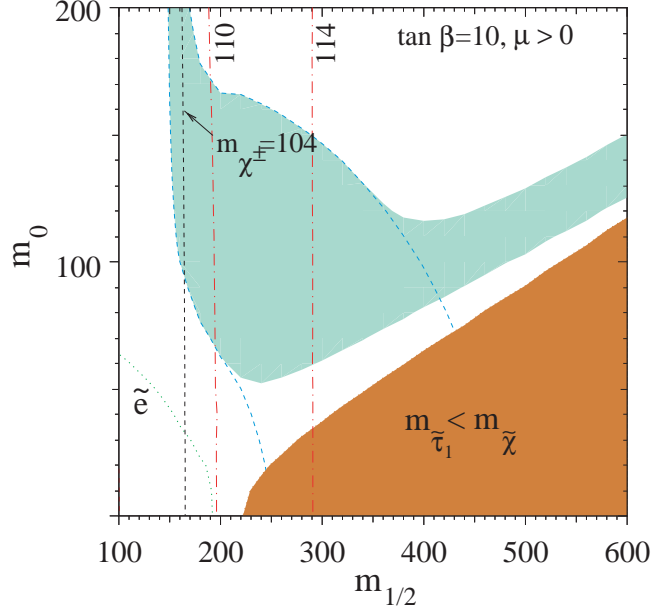


Figure 13. The light-shaded 'bulk' area is the cosmologically preferred region with  $0.1 < h^2 < 0.3$ . The light dashed lines show the location of the cosmologically preferred region if one ignores coannihilations with the light sleptons. In the dark shaded region in the bottom right, the LSP is the  $\tilde{\chi}_1^0$ , leading to an unacceptable abundance of charged dark matter. Also shown is the isomass contour  $m_{\tilde{\chi}^\pm} = 104$  GeV and  $m_h = 110, 114$  GeV, as well as an indication of the slepton bound from LEP.

The constraint imposed by measurements of  $b \bar{b} \rightarrow s \bar{s}$  <sup>129</sup> also exclude small values of  $m_{1/2}$ . These measurements agree with the Standard Model, and therefore provide bounds on MSSM particles, such as the chargino and charged Higgs masses, in particular. Typically, the  $b \bar{b} \rightarrow s \bar{s}$  constraint is more important for  $\tan \beta < 0$ , but it is also relevant for  $\tan \beta > 0$ , particularly when  $\tan \beta$  is large. The BNL E821 experiment reported last year a new measurement of a  $\frac{1}{2} g_F(2)$  which deviated by 2.6 standard deviations from the best Standard Model prediction available at that time <sup>130</sup>. However, it had been realized that the sign of the most important pseudoscalar meson pole part of the light-by-light scattering contribution <sup>131</sup> to the Standard Model prediction should be reversed, which reduces the apparent experimental discrepancy to about 1.6 standard deviations ( $a = 10^{10} = 26 \pm 16$ ). The largest contribution to the errors in the comparison with theory was

thought to be the statistical error of the experiment, which has been significantly reduced just recently<sup>132</sup>. The world average of  $a_{1/2}^1 (g = 2)$  now deviates by  $(33.9 \pm 11.2) \times 10^{-10}$  from the Standard Model calculation of Davier et al.<sup>133</sup> using  $e^+ e^-$  data, and by  $(17 \pm 11) \times 10^{-10}$  from the Standard Model calculation of Davier et al.<sup>133</sup> based on decay data. Other recent analyses of the  $e^+ e^-$  data yield similar results. On the subsequent plots, the form  $a_{1/2}^1$  range  $11.5 \times 10^{-10} < a < 56.3 \times 10^{-10}$  is displayed.

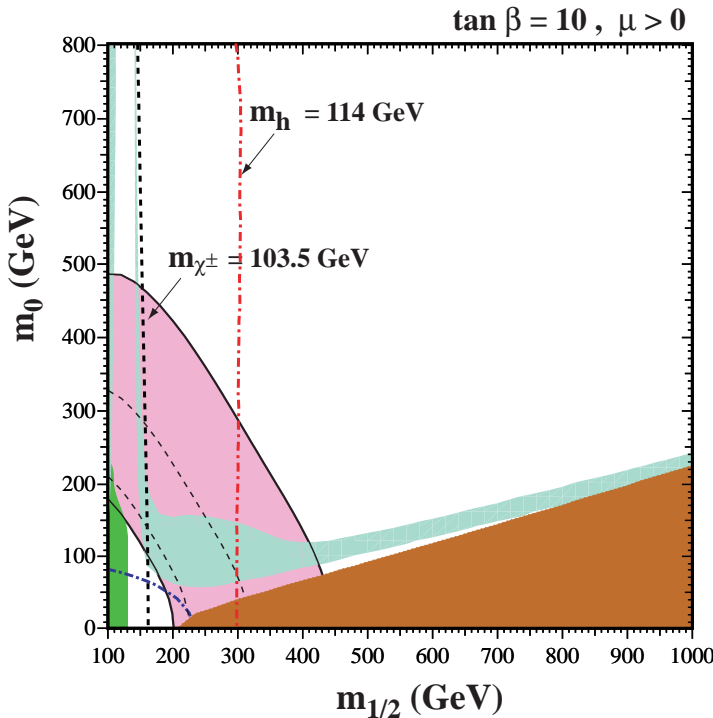


Figure 14. Compilation of phenomenological constraints on the CM SSM for  $\tan \beta = 10$ ;  $\mu > 0$ , assuming  $A_0 = 0$ ;  $m_t = 175$  GeV and  $m_b (m_b)_{SM}^{MS} = 4.25$  GeV. The near-vertical lines are the LEP limits  $m_{\tilde{\chi}^0} = 103.5$  GeV (dashed and black)<sup>119</sup>, and  $m_{\tilde{h}} = 114.1$  GeV (dotted and red)<sup>128</sup>. Also, in the lower left corner we show the  $m_{\tilde{\chi}^0} = 99$  GeV contour<sup>135</sup>. In the dark (brick red) shaded regions, the LSP is the charged  $\tilde{\chi}^{\pm}$ , so this region is excluded. The light (turquoise) shaded areas are the cosmologically preferred regions with  $0.1 < h^2 < 0.3$ <sup>125</sup>. The medium (dark green) shaded regions are excluded by  $b \neq 129$ . The shaded (pink) region in the upper right delineates the  $g = 2$  range of  $g = 2$ . The dashed curves within this region correspond to the 1-sigma bounds.

Following a previous analysis<sup>125,134</sup>, in Figure 14 the  $m_{1=2}$  –  $m_0$  parameter space is shown for  $\tan\beta = 10$ . The dark shaded region (in the lower right) corresponds to the parameters where the LSP is not a neutralino but rather a  $\tilde{\chi}_R^0$ . The cosmologically interesting region at the left of the figure is due to the appearance of pole effects. There, the LSP can annihilate through s-channel  $Z$  and  $h$  (the light Higgs) exchange, thereby allowing a very large value of  $m_0$ . However, this region is excluded by phenomenological constraints. Here one can see clearly the coannihilation tail which extends towards large values of  $m_{1=2}$ . In addition to the phenomenological constraints discussed above, Figure 14 also shows the current experimental constraints on the CM SSM parameter space due to the limit  $m_h > 103.5$  GeV provided by chargino searches at LEP<sup>119</sup>. LEP has also provided lower limits on slepton masses, of which the strongest is  $m_{\tilde{e}} > 99$  GeV<sup>135</sup>. This is shown by dot-dashed curve in the lower left corner of Fig. 14. Similar results have been found by other analyses<sup>136</sup>.

As one can see, one of the most important phenomenological constraint at this value of  $\tan\beta$  is due to the Higgs mass (shown by the nearly vertical dot-dashed curve). The theoretical Higgs masses were evaluated using FeynHiggs<sup>137</sup>, which is estimated to have a residual uncertainty of a couple of GeV in  $m_h$ . The region excluded by the  $m_h$  constraint is the dark shaded (green) region to the left of the plot. As many authors have pointed out<sup>138</sup>, a discrepancy between theory and the BNL experiment could well be explained by supersymmetry. As seen in Fig. 14, this is particularly easy if  $\tan\beta > 0$ . The medium (pink) shaded region in the figure corresponds to the overall allowed region (2) by the new experimental result.

As discussed above, another mechanism for extending the allowed CM SSM region to large  $m_0$  is rapid annihilation via a direct-channel pole when  $m_0 > \frac{1}{2}m_A$ <sup>124,125</sup>. This may yield a ‘funnel’ extending to large  $m_{1=2}$  and  $m_0$  at large  $\tan\beta$ , as seen in Fig. 15.

In principle, the true input parameters in the CM SSM are:  $m_1, m_2$ ; and  $B$ , where  $m_1$  and  $m_2$  are the Higgs soft masses (in the CM SSM  $m_1 = m_2 = m_0$  and  $B$  is the susy breaking bilinear mass term). In this case, the electroweak symmetry breaking conditions lead to a prediction of  $M_Z, \tan\beta$ , and  $m_A$ . Since we are not really interested in predicting  $M_Z$ , it is more useful to assume instead the following CM SSM input parameters:  $M_Z, m_1, m_2$ ; and  $\tan\beta$  again with  $m_1 = m_2 = m_0$ . In this case, one predicts  $B$ , and  $m_A$ . However, one can generalize the CM SSM case to include non-universal Higgs masses<sup>139,140</sup> (NUHM), in which case the

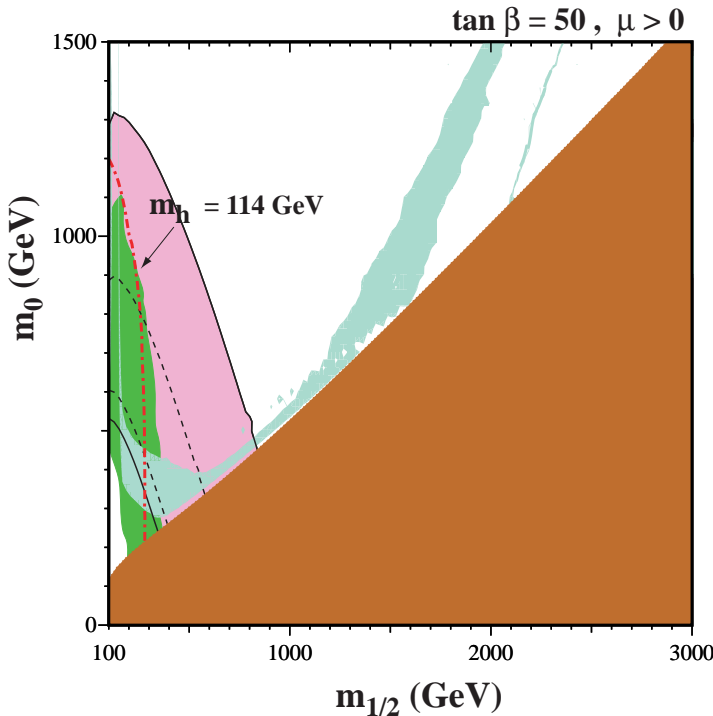


Figure 15. As in Fig. 14 for  $\tan \beta = 50$ .

input parameters become  $M_Z$ ;  $m_A$ ; and  $\tan \beta$  and one predicts  $m_1$ ;  $m_2$ , and  $B$ .

The NUHM parameter space was recently analyzed<sup>140</sup> and a sample of the results found is shown in Fig. 16. While much of the cosmologically preferred area with  $\mu < 0$  is excluded, there is a significant enhancement in the allowed parameter space for  $\mu > 0$ .

### 3.5. Detection

Because the LSP as dark matter is present locally, there are many avenues for pursuing dark matter detection. Direct detection techniques rely on an ample neutralino-nucleon scattering cross-section. The effective four-fermion lagrangian can be written as

$$L = \bar{q}_i^5 \bar{q}_i^5 ( \bar{q}_1^i + \bar{q}_2^i + \bar{q}_3^i + \bar{q}_4^i ) + \bar{q}_1^i \bar{q}_1^i + \bar{q}_2^i \bar{q}_2^i + \bar{q}_3^i \bar{q}_3^i + \bar{q}_4^i \bar{q}_4^i$$

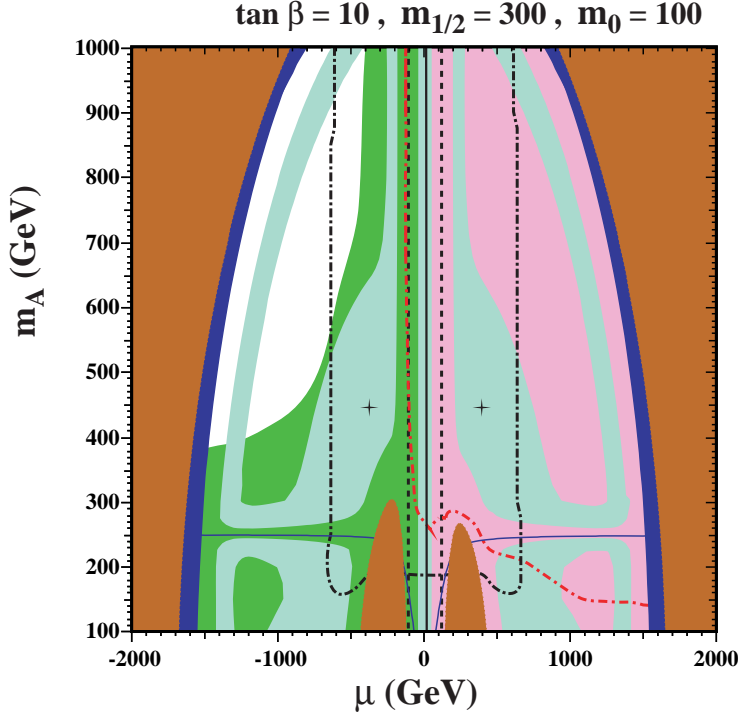


Figure 16. Compilations of phenomenological constraints on the MSSM with NUHM in the  $(\mu, m_A)$  plane for  $\tan \beta = 10$  and  $m_0 = 100$  GeV,  $m_{1/2} = 300$  GeV, assuming  $A_0 = 0$ ,  $m_t = 175$  GeV and  $m_b (m_b)^{\overline{MSM}} = 425$  GeV. The shading is as described in Fig. 14. The (blue) solid line is the contour  $m_A = 200$  GeV, near which rapid direct-channel annihilation suppresses the relic density. The dark (black) dot-dashed line indicates when one or another Higgs mass-squared becomes negative at the GUT scale: only lower  $jj$  and larger  $m_A$  values are allowed. The crosses denote the values of  $\mu$  and  $m_A$  found in the CMSSM.

$$+ \quad 5i \quad q_1 \quad 5 \quad q_1 + \quad 6i \quad 5 \quad q_1 q_1 \quad (59)$$

However, the terms involving  $1i$ ,  $4i$ ,  $5i$ , and  $6i$  lead to velocity dependent elastic cross sections. The remaining terms are: the spin dependent coefficient,  $2i$  and the scalar coefficient  $3i$ . Contributions to  $2i$  are predominantly through light squark exchange. This is the dominant channel for binos. Scattering also occurs through  $Z$  exchange but this channel requires a strong Higgsino component. Contributions to  $3i$  are also dominated by light squark exchange but Higgs exchange is non-negligible in most cases.

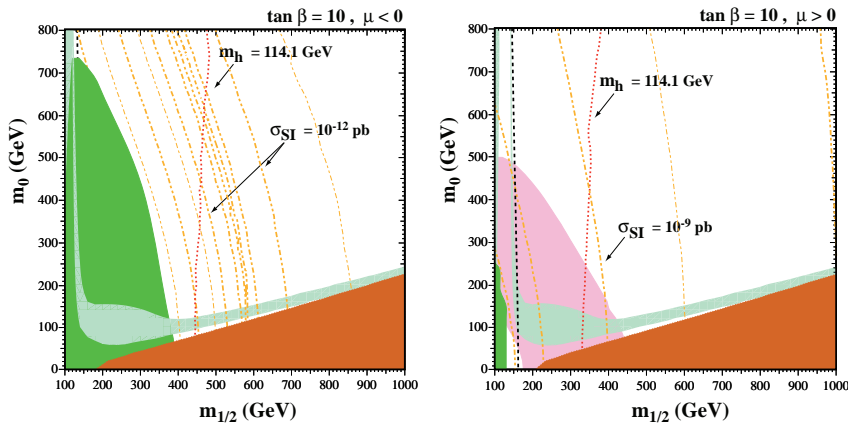


Figure 17. Spin-independent cross sections in the  $(m_{1/2}, m_0)$  planes for (a)  $\tan \beta = 10$ ,  $\mu < 0$ , (b)  $\tan \beta = 10$ ,  $\mu > 0$ . The double dot-dashed (orange) curves are contours of the spin-independent cross section, differing by factors of 10 (bolder) and interpolating factors of 3 (nearer when shown). For example, in (b), the curves to the right of the one marked  $10^{-9}$  pb correspond to  $3 \times 10^{-10}$  pb and  $10^{-10}$  pb.

Fig. 17 displays contours of the spin-independent cross section for the elastic scattering of the LSP on protons in the  $m_{1/2}, m_0$  planes for (a)  $\tan \beta = 10$ ,  $\mu < 0$ , (b)  $\tan \beta = 10$ ,  $\mu > 0$ <sup>141</sup>. The double dot-dashed (orange) lines are contours of the spin-independent cross section, and the contours  $\sigma_{SI} = 10^{-9}$  pb in panel (a) and  $\sigma_{SI} = 10^{-12}$  pb in panel (b) are indicated. The LEP lower limits on  $m_h$  and  $m_0$ , as well as the experimental measurement of  $b_1$  for  $\mu < 0$ , tend to bound the cross sections from above, as discussed in more detail below. Generally speaking, the spin-independent cross section is relatively large in the 'bulk' region, but falls off in the coannihilation 'tail'. Also, we note also that there is a strong cancellation in the spin-independent cross section when  $\mu < 0$ <sup>142,143</sup>, as seen along strips in panel (a) of Fig. 17 where  $m_{1/2} > 500$  GeV. In the cancellation region, the cross section drops lower than  $10^{-14}$  pb. All these possibilities for suppressed spin-independent cross sections are disfavoured by the data on  $g_F = 2$ , which favour values of  $m_{1/2}$  and  $m_0$  that are not very large, as well as  $\mu > 0$ , as seen in panel (b) of Fig. 17. Thus  $g_F = 2$  tends to provide a lower bound on the spin-independent cross section.

Fig. 18 (a) illustrates the effect on the cross sections of each of the principal phenomenological constraints, for the particular case  $\tan \beta = 10$ ,  $\mu > 0$ . The solid (blue) lines mark the bounds on the cross sections allowed by

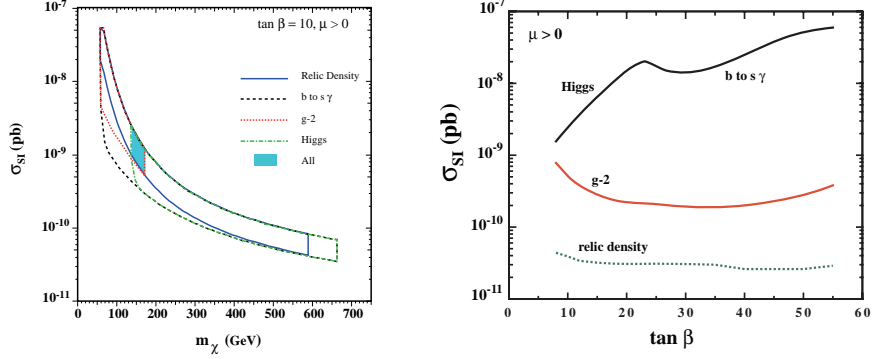


Figure 18. Allowed ranges of the cross sections for  $\tan \beta = 10$  (a)  $\mu > 0$  for spin-independent elastic scattering. The solid (blue) lines indicate the relic density constraint, the dashed (black) lines the  $b \rightarrow s\gamma$  constraint, the dot-dashed (green) lines the  $m_h$  constraint, and the dotted (red) lines the  $g-2$  constraint. The shaded (pale blue) region is allowed by all the constraints. (b) The allowed ranges of the spin-independent cross section for  $\mu > 0$ . The darker solid (black) lines show the upper limits on the cross sections obtained from  $m_h$  and  $b \rightarrow s\gamma$ , and (where applicable) the lighter solid (red) lines show the lower limits suggested by  $g-2$  and the dotted (green) lines the lower limits from the relic density.

the relic-density constraint  $0.1 < m_{1=2}^2 < 0.3$  alone. For any given value of  $m_{1=2}$ , only a restricted range of  $m_0$  is allowed. Therefore, only a limited range of  $m_0$ , and hence only a limited range for the cross section, is allowed for any given value of  $m_{1=2}$ . The thicknesses of the allowed regions are due in part to the assumed uncertainties in the nuclear inputs. These have been discussed at length in 143;142. On the other hand, a broad range of  $m_0$  is allowed, when one takes into account the coannihilation 'tail' region at each  $\tan \beta$  and the rapid-annihilation 'funnel' regions for  $\tan \beta = 35, 50$ . The dashed (black) line displays the range allowed by the  $b \rightarrow s\gamma$  constraint alone. In this case, a broader range of  $m_0$  and hence the spin-independent cross section is possible for any given value of  $m_{1=2}$ . The impact of the constraint due to  $m_h$  is shown by the dot-dashed (green) line. Comparing with the previous constraints, we see that a region at low  $m_0$  is excluded by  $m_h$ , strengthening significantly the previous upper limit on the spin-independent cross section. Finally, the dotted (red) lines in Fig. 18 show the impact of the  $g-2$  constraint. This imposes an upper bound on  $m_{1=2}$  and hence  $m_0$ , and correspondingly a lower limit on the spin-independent cross section.

This analysis is extended in panel (b) of Fig. 18 to all the values  $8 <$

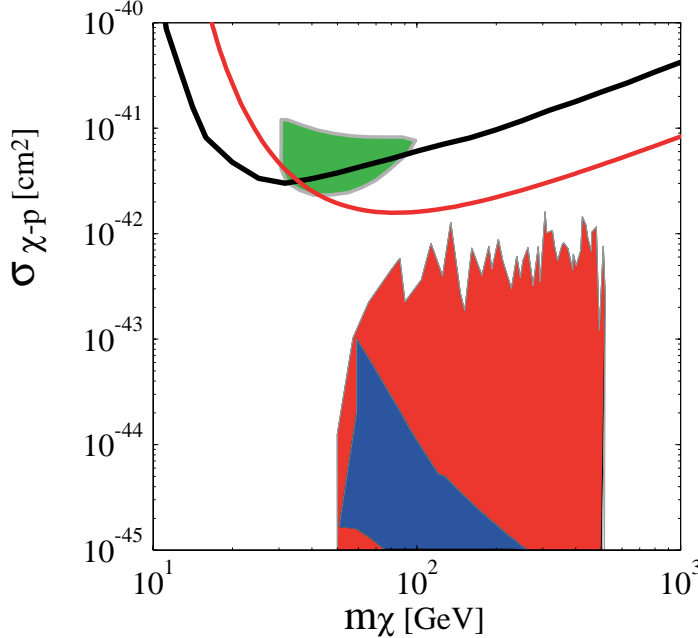


Figure 19. Limits from the CDM S<sup>145</sup> and Edelweiss<sup>146</sup> experiments on the neutralino-proton elastic scattering cross section as a function of the neutralino mass. The Edelweiss limit is stronger at higher  $m_\chi$ . These results nearly exclude the shaded region observed by DAMA<sup>147</sup>. The theoretical predictions lie at lower values of the cross section.

$\tan \beta = 55$  and we find overall that<sup>141</sup>

$$2 \times 10^{-10} \text{ pb} < \sigma_{SI} < 6 \times 10^{-8} \text{ pb}; \quad (60)$$

$$2 \times 10^{-7} \text{ pb} < \sigma_{SD} < 10^{-5} \text{ pb}; \quad (61)$$

for  $\tan \beta > 0$ . ( $\sigma_{SD}$  is the spin-dependent cross-section not shown in the figures presented here.) As we see in panel (b) of Fig. 18,  $m_h$  provides the most important upper limit on the cross sections for  $\tan \beta < 23$ , and  $b \neq s$  for larger  $\tan \beta$ , with  $g = 2$  always providing a more stringent lower limit than the relic-density constraint. The relic density constraint shown is evaluated at the endpoint of the coannihilation region. At large  $\tan \beta$ , the Higgs funnels or the focus-point regions have not been considered, as their locations are very sensitive to input parameters and calculational details<sup>144</sup>.

The results from a CMSSM and MSSM analysis<sup>142,143</sup> for  $\tan \beta = 3$

and 10 are compared with the most recent CDM S<sup>145</sup> and Edelweiss<sup>146</sup> bounds in Fig. 19. These results have nearly entirely excluded the region purported by the DAMA<sup>147</sup> experiment. The CM SSM prediction<sup>142</sup> is shown by the dark shaded region, while the NUHM case<sup>143</sup> is shown by the larger lighter shaded region. Other CM SSM results<sup>148</sup> are also available.

I conclude by showing the prospects for direct detection for the benchmark points discussed above<sup>149</sup>. Fig. 20 shows rates for the elastic spin-independent scattering of supersymmetric relics, including the projected sensitivities for CDM S II<sup>150</sup> and CRESST<sup>151</sup> (solid) and GENIUS<sup>152</sup> (dashed). Also shown are the cross sections calculated in the proposed benchmark scenarios discussed in the previous section, which are considerably below the DAMA<sup>147</sup> range ( $10^{-5} - 10^{-6}$  pb). Indirect searches for supersymmetric dark matter via the products of annihilations in the galactic halo or inside the Sun also have prospects in some of the benchmark scenarios<sup>149</sup>.

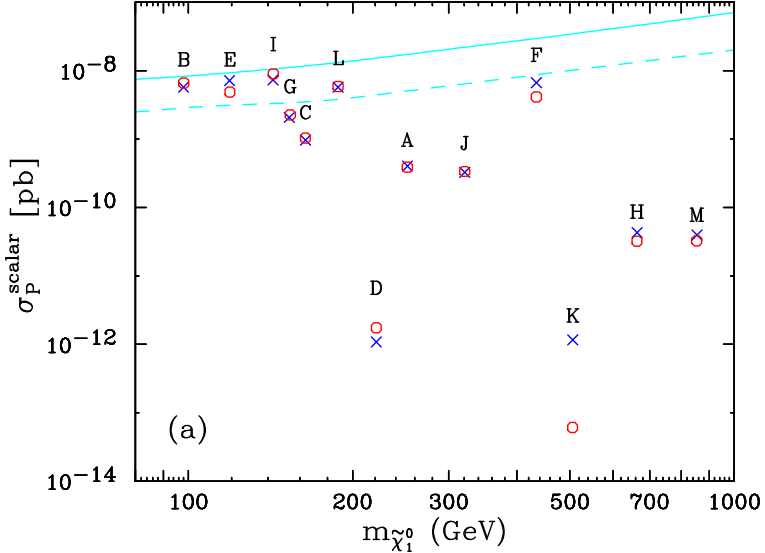


Figure 20. Elastic spin-independent scattering of supersymmetric relics on protons calculated in benchmark scenarios<sup>149</sup>, compared with the projected sensitivities for CDM S II<sup>150</sup> and CRESST<sup>151</sup> (solid) and GENIUS<sup>152</sup> (dashed). The predictions of our code (blue crosses) and Neutdriver<sup>153</sup> (red circles) for neutralino-nucleon scattering are compared. The labels A, B, ..., L correspond to the benchmark points as shown in Fig. 12.

## References

1. F. Zwicky, *Helv. Phys. Acta* 6 (1933) 110.
2. S. Folkes et al., *MNRAS* 308 (1999) 459; M. L. B. Lanton et al., *Astr. J.* 121 (2001) 2358.
3. S. M. Faber and J. J. Gallagher, *Ann. Rev. Astron. Astrophys.* 17 (1979) 135.
4. A. Bosma, *Ap. J.* 86 (1981) 1825; V. C. Rubin, W. K. Ford and N. Thonnard, *Ap. J.* 238 (1980) 471; V. C. Rubin, D. Burstein, W. K. Ford and N. Thonnard, *Ap. J.* 289 (1985) 81; T. S. Van Albada and R. Sancisi, *Phil. Trans. R. Soc. Land. A* 320 (1986) 447.
5. M. Persic and P. Salucci, *Ap. J. Supp.* 99 (1995) 501; M. Persic, P. Salucci, and F. Stel, *MNRAS* 281 (1996) 27P.
6. R. P. Saglia et al., *Ap. J.* 403 (1993) 567; C. M. Carollo et al., *Ap. J.* 411 (1995) 25; A. Bonriello, P. Salucci, and L. D'aneese, [astro-ph/0208268](#).
7. D. Fabricant and P. Gorenstein, *Ap. J.* 267 (1983) 535; G. C. Stewart, C. R. Canizares, A. C. Fabian and P. E. J. Nielsen, *Ap. J.* 278 (1984) 53 and references therein.
8. W. Forman, C. Jones, and W. Tucker, *Ap. J.* 293 (1985) 102; A. C. Fabian, P. A. Thompson, S. M. Fall, and R. E. White III, *MNRAS* 221 (1986) 1049; M. Loewenstein and R. E. White, *Ap. J.* 518 (1999) 50; M. Loewenstein and R. F. M. Ushotzky, [astro-ph/0208090](#).
9. R. M. Ushotzky, in *Relativistic Astrophysics and Particle Cosmology* ed. C. W. Akerlof and M. Srednicki (New York Academy of Sciences, New York, 1993), p. 184; J. S. Mulchaey, D. S. Davids, R. F. M. Ushotzky, and D. Burstein, *Ap. J.* 404 (1993) L9; M. J. Henriksen and G. A. Mamon, *Ap. J.* 421 (1994) L63; L. P. David, C. Jones, and W. Forman, *Ap. J.* 445 (1995) 578.
10. S. D. M. White, J. F. Navarro, A. E. Evrard, and C. S. Frenk, *Nature* 366 (1993) 429; S. Schindler, *A. A.* 305 (1996) 756.
11. J. A. Tyson, F. Valdes, and R. A. Wenk, *Ap. J.* 349 (1990) L1.
12. E. Turner, J. Ostriker, and J. Gott III, *Ap. J.* 284 (1984) 1.
13. G. G. Olsøe, J.-P. Kneib, and G. Soucail, *A. A.* 387 (2002) 788.
14. R. Blanford and R. Narayan, *Ann. Rev. A. A.* 30 (1992) 311.
15. P. Fischer et al., *Astr. J.* 120 (2000) 1198; D. Smith, G. Bernstein, P. Fischer, and M. Jarvis, *Ap. J.* 551 (2001) 641; N. Straumann, *Sp. Sci. Rev.* 100 (2002) 29.
16. Y. M. Ellier, *Ann. Rev. Astr. Astr.* 37 (1999) 127.
17. L. van Waerbeke, Y. M. Ellier, and M. Radovich, *A. A.* 374 (2001) 757.
18. T. Erben et al., *A. A.* 355 (2000) 23; K. Umetsu and T. Futamase, *Ap. J.* 539 (2000) 5; H. Bonnet, Y. M. Ellier, and B. Fort, *Ap. J.* 427 (1994) L83.
19. Y. M. Ellier, *Sp. Sci. Rev.* 100 (2002) 73.
20. P. J. E. Peebles, *The Large Scale Structure of the Universe*, (Princeton University Press, Princeton, 1980).
21. A. D. Ressler, D. Lynden-Bell, D. Burstein, R. Davids, S. Faber, R. Terlevich, and G. Wegner, *Ap. J.* 313 (1987) L37; A. Dekel, E. Bertschinger, A. Yahil, M. A. Strauss, M. Davids, and J. P. Huchra, *Ap. J.* 412 (1993) 1.
22. J. A. Willick, M. A. Strauss, A. Dekel, and T. K. Olatt, *Ap. J.* 486 (1997) 629;

J.A. Willcock and M.A. Strauss, *A&A* 307 (1998) 64.

23. Y. Srigad, A. Eddar, A. Dekel, M.A. Strauss, and A. Yahil, *Ap.J.* 495 (1998) 516; E. Branchini, I. Zehavi, M. Plionis, and A. Dekel, *MNRAS* 313 (2000) 491.

24. S. Schindler, *Sp. Sci. Rev.* 100 (2002) 299.

25. R.A. Alpher and R.C. Herman, *Phys. Rev.* 74, 1737 (1948); *Phys. Rev.* 75, 1089 (1949).

26. A.T. Lee et al., *Ap.J.* 561 (2001) L1 [[arXiv:astro-ph/0104459](#)].

27. C.B. Netterfield et al. [Boomerang Collaboration], *Ap.J.* 571 (2002) 604 [[arXiv:astro-ph/0104460](#)].

28. N.W. Halverson et al. *MNRAS* 568 (2002) 38 [[arXiv:astro-ph/0104489](#)].

29. R. Stompor et al., *Ap.J.* 561 (2001) L7 [[arXiv:astro-ph/0105062](#)].

30. C. Pryke, N.W. Halverson, E.M. Leitch, J. Kovac, J.E. Carlstrom, W.L. Holzapfel and M. Dragovan, *Ap.J.* 568 (2002) 46 [[arXiv:astro-ph/0104490](#)].

31. S. Padin, et al. *Ap.J.* 549 (2001) L1.

32. J.A. Rubino-Martin et al., [arXiv:astro-ph/0205367](#).

33. A. Benoit et al. [Archeops Collaboration], [arXiv:astro-ph/0210306](#).

34. M.E. Abroë et al., *MNRAS* 334 (2002) 11 [[arXiv:astro-ph/0111010](#)].

35. W.L. Freedman et al., *Ap.J.* 553 (2001) 47.

36. A.G. Riess et al., *A.J.* 116 (1998) 1009; S. Perlmutter et al., *Ap.J.* 517 (1999) 565; A.G. Riess, *PASP* 112 (2000) 1284.

37. K.A. Olive and J.A. Peacock, *Phys. Rev. D* 66 (2002) 010001.

38. for reviews see: A.D. Linde, *Particle Physics And Inflationary Cosmology* Harwood (1990); K.A. Olive, *Phys. Rep.* 190 (1990) 307; D.H. Lyth and A.Riotto, *Phys. Rept.* 314 (1999) 1 [[arXiv:hep-ph/9807278](#)].

39. W.H. Press, *Phys. Scr.* 21 (1980) 702; V.F. Mukhanov and G.V. Chibisov, *JETP Lett.* 33 (1981) 532; S.W. Hawking, *Phys. Lett.* 115B (1982) 295; A.A. Starobinsky, *Phys. Lett.* 117B (1982) 175; A.H. Guth and S.Y. Pi, *Phys. Rev. Lett.* 49 (1982) 1110; J.M. Bardeen, P.J. Steinhardt and M.S. Turner, *Phys. Rev. D* 28 (1983) 679.

40. E.R. Harrison, *Phys. Rev. D* 1 (1979) 2726; Ya.B. Zeldovich, *MNRAS* 160 (1972) 1P.

41. E.L. Wright et al. *Ap.J.* 396 (1992) L13; G.H. Hinshaw et al., *Ap.J.* 464 (1996) L17; G.F. Smoot and D. Scott, *Phys. Rev. D* 66 (2002) 010001.

42. J.R. Bond and A.S. Szalay, *Ap.J.* 274 (1983) 443.

43. J.R. Bond, G. Efstathiou and J. Silk, *Phys. Lett.* 45 (1980) 1980; Ya.B. Zeldovich and R.A. Sunyaev, *Sov. Astr. Lett.* 6 (1980) 457.

44. T.P. Walker, G. Steigman, D.N. Schramm, K.A. Olive and K. Kang, *Ap.J.* 376 (1991) 51; S. Sarkar, *Rep. Prog. Phys.* 59 (1996) 1493; K.A. Olive, G. Steigman, and T.P. Walker, *Phys. Rep.* 333 (2000) 389; B.D. Fields and S. Sarkar, *Phys. Rev. D* 66 (2002) 010001.

45. L.M. Krauss and P. Romanelli, *Ap.J.* 358 (1990) 47; M. Smit, L. Kawano, and R.A. Malaney, *Ap.J. Supp.* 85 (1993) 219; N. Hata, R.J. Scherrer, G. Steigman, D. Thomas, and T.P. Walker, *Ap.J.* 458 (1996) 637; A. Coc, E. Vangioni-Flam, M. Casse and M. Rabiet, *Phys. Rev. D* 65

(2002) 043510; K. M. Nollett and S. Burles, Phys. Rev. D 61 (2000) 123505 [arX iv:astro-ph/0001440].

46. R. H. Cyburt, B. D. Fields, and K. A. Olive, New Ast. 6 (1996) 215 [arX iv:astro-ph/0102179].
47. B. D. Fields and K. A. Olive, Ap. J. 506 (1998) 177 [arX iv:astro-ph/9803297].
48. K. A. Olive, and E. Skillman, New Ast. 6 (2001) 119 [arX iv:astro-ph/0007081].
49. Y. I. Izotov and T. X. Thuan, Ap. J. 500 (1998) 188; Y. I. Izotov, T. X. Thuan, and V. A. Lipovetsky, Ap. J. 108 (1997) 1; Y. I. Izotov, T. X. Thuan, and V. A. Lipovetsky, Ap. J. 435 (1994) 647.
50. M. Peimbert, A. Peimbert and M. T. Ruiz, Ap. J. 541 (2000) 688; A. Peimbert, M. Peimbert and V. Luridiana, Ap. J. 565 (2002) 668.
51. S. G. Ryan et al., Ap. J. 523 (2000) L57.
52. P. Bonifacio, et al., A. A. 390 (2002) 91.
53. J. M. O'Meara, D. Tytler, D. Kirkman, N. Suzuki, J. X. Prochaska, D. Lubin and A. M. Wolfe, Ap. J. 552 (2001) 718 [arX iv:astro-ph/0011179].
54. D. Tytler, J. M. O'Meara, N. Suzuki, and D. Lubin, Phys. Rep. 333 (2000) 409.
55. M. Pettini and D. V. Bowen, Ap. J. 560 (2001) 41 [arX iv:astro-ph/0104474]; S. D'Odorico, M. D'essauges-Zavadsky, and P. Molinaro, A. A. 368 (2001) L21.
56. B. D. Fields, K. A. Olive, J. Silk, M. Casse and E. Vangioni-Flam, Ap. J. 563 (2001) 653 [arX iv:astro-ph/0107389].
57. H. Reeves, J. Audouze, W. Fowler, and D. N. Schramm, Ap. J. 179 (1976) 909.
58. T. M. Bania, R. T. Rood and D. S. Balser, Nature 415 (2002) 54.
59. E. Vangioni-Flam, K. A. Olive, B. D. Fields and M. Casse, arX iv:astro-ph/0207583.
60. M. Persic and P. Salucci, MNRAS 258 (1992) 14p.
61. M. Fukugita, C. J. Hogan, and P. J. E. Peebles, Ap. J. 503 (1998) 518.
62. M. G. Haehnelt, P. Madau, R. Kudritzki, and F. Haardt, Ap. J. 549 (2001) L151; D. Reimers, Sp. Sci. Rev. 100 (2002) 89.
63. D. J. Hegyi and K. A. Olive, Phys. Lett. 126B (1983) 28; Ap. J. 303 (1986) 56.
64. C. Low and D. Lynden-Bell, MNRAS 176 (1976) 367; M. J. Reeves, MNRAS 176 (1976) 483; J. Silk, Ap. J. 256 (1982) 514; F. Palla, E. E. Salpeter and S. W. Stahler, Ap. J. 271 (1983) 632.
65. J. M. Scalo, Fund. Comm. Phys. 11 (1986) 1.
66. D. J. Hegyi and G. L. Gerber, Ap. J. 218 (1987) L7; D. J. Hegyi, in Proc. of 1st Michigan Astrophysics Meeting, Audouze, P. Crane, D. Hegyi, and J. Tran. Than Van, eds., (Dreux, FranceFrontiers) 1981, p. 321; S. P. Boughn, P. R. Saulson, and M. Seldner, Ap. J. 250 (1981) L15.
67. B. Paczynski, Ap. J. 304 (1986) 1.
68. C. Alcock et al., Nature 365 (1993) 621; E. Aubourg et al. Nature 365 (1993) 623.
69. C. Alcock et al., Ap. J. 542 (2000) 281.
70. T. Lasserre, et al., A. A. 355 (2000) 39L; C. Afonso et al., astro-ph/0212176.

71. B.J.Carr, *Ann. Rev. Astron. Astrophys.* 32 (1994) 531; [astro-ph/0102389](#).

72. D.S.Ryu, K.A.Olive and J.Silk, *Ap. J.* 353 (1990) 81.

73. B.D.Fields, K.Freese, and D.S.Graf, *Ap. J.* 534 (2000) 265.

74. J.H.MacGibbon, *Nature* 329 (1987) 308.

75. B.J.Carr, J.R.Bond and W.D.Amett, *Ap. J.* 277 (1984) 445; J.R.Bond, W.D.Amett and B.J.Carr, *Ap. J.* 280 (1984) 825; W.W.Ober, M.F.ElEid and K.J.Fricke, *A. A.* 119 (1983) 61.

76. C.G.Lacey, and J.P.Ostriker, *Ap. J.* 299 (1985) 633.

77. H.W.Rix and G.Lake, *Ap. J.* 417 (1993) L1.

78. D.N.Schramm and G.Steigman, *Ap. J.* 243 (1981) 1.

79. P.J.E.Peebles, *Ap. J.* 258 (1982) 415; A.Melott, *MNRAS* 202 (1983) 595; *A. A.* Klypin, S.F.Shandarin, *MNRAS* 204 (1983) 891.

80. C.S.Frenk, S.D.M.White and M.Davis, *Ap. J.* 271 (1983) 417.

81. S.D.M.White, C.S.Frenk and M.Davis, *Ap. J.* 274 (1983) 61.

82. J.R.Bond, J.Centrella, A.S.Szalay and J.Wilson, in *Formation and Evolution of Galaxies and Large Structures in the Universe*, ed. J.Andouze and J.Tran Thanh Van, (Dordrecht-Reidel 1983) p.87.

83. K.Enqvist, K.Kainulainen and V.Semikoz, *Nucl. Phys. B* 374 (1992) 392.

84. S.S.Gerstein and Ya.B.Zeldovich, *JETP Lett.* 4 (1966) 647; R.Cowsik and J.M.C.Kelland, *Phys. Rev. Lett.* 29 (1972) 669; A.S.Szalay and G.Marx, *A. A.* 49 (1976) 437.

85. K.Kainulainen and K.A.Olive, [arXiv:hep-ph/0206163](#).

86. R.A.Croft, W.Hu and R.Dave, *Phys. Rev. Lett.* 83 (1999) 1092 [[arXiv:astro-ph/9903335](#)].

87. X.M.Wang, M.Tegmark and M.Zaldarriaga, *Phys. Rev. D* 65 (2002) 123001 [[arXiv:astro-ph/0105091](#)].

88. E.Elgaroy et al., *Phys. Rev. Lett.* 89 (2002) 061301 [[arXiv:astro-ph/0204152](#)].

89. A.Lewis and S.Bridle, *Phys. Rev. D* 66 (2002) 103511 [[arXiv:astro-ph/0205436](#)].

90. P.Hut, *Phys. Lett. B* 69 (1977) 85; B.W.Lee and S.Weinberg, *Phys. Rev. Lett.* 39 (1977) 165; M.I.Vysotsky, A.D.Dolgov and Y.B.Zeldovich, *Pisma Zh. Eksp. Teor. Fiz.* 26 (1977) 200.

91. E.W.Kolb and K.A.Olive, *Phys. Rev. D* 33 (1986) 1202; *E*:34 (1986) 2531; L.M.Krauss, *Phys. Lett.* 128B (1983) 37.

92. R.Watkins, M.Srednicki and K.A.Olive, *Nucl. Phys. B* 310 (1988) 693.

93. K.Enqvist, K.Kainulainen and J.Maalaampi, *Nucl. Phys. B* 317 (1989) 647.

94. K.Enqvist and K.Kainulainen, *Phys. Lett. B* 264 (1991) 367.

95. K.Griest and M.Kamionkowski, *Phys. Rev. Lett.* 64 (1990) 615.

96. P.Hut and K.A.Olive, *Phys. Lett. B* 87 (1979) 144.

97. D.Abbaneo et al. [ALEPH Collaboration], [arXiv:hep-ex/0112021](#).

98. S.Ahlen, et al., *Phys. Lett. B* 195 (1987) 603; D.D.Caldwell, et al., *Phys. Rev. Lett.* 61 (1988) 510; M.Beck et al., *Phys. Lett. B* 336 (1994) 141.

99. Ch.Weinheimer, et al., *Phys. Lett. B* 460 (1999) 219.

100. G.Steigman, K.A.Olive, and D.N.Schramm, *Phys. Rev. Lett.* 43 (1979) 239; K.A.Olive, D.N.Schramm, and G.Steigman, *Nucl. Phys. B* 180 (1981)

497.

101. K. A. Olive and M. S. Turner, *Phys. Rev. D* 25 (1982) 213.
102. S. H. Hansen, J. Lesgourges, S. Pastor and J. Silk, *MNRAS* 333 (2002) 544 [[arXiv:astro-ph/0106108](#)].
103. R. D. Peccei and H. R. Quinn, *Phys. Rev. Lett.* 37 (1977) 1440; *Phys. Rev. D* 16 (1977) 1791; S. Weinberg, *Phys. Rev. Lett.* 40 (1978) 223; F. Wilczek, *Phys. Rev. Lett.* 40 (1978) 279.
104. J. E. Kim, *Phys. Rev. Lett.* 43 (1979) 103; M. A. Shifman, A. I. Vainshtein, and V. I. Zakharov, *Nucl. Phys. B* 166 (1980) 493; M. Dine, W. Fischler, and M. Srednicki, *Phys. Lett.* 104B (1981) 199.
105. J. Preskill, M. B. Wise, and F. Wilczek, *Phys. Lett.* 120B (1983) 127; L. F. Abbott and P. Sikivie, *Phys. Lett.* 120B (1983) 133; M. Dine and W. Fischler, *Phys. Lett.* 120B (1983) 137.
106. G. Racliet, *Phys. Rep.* 198 (1990) 1.
107. D. D. Dearborn, D. N. Schramm, and G. Steigman, *Phys. Rev. Lett.* 56 (1986) 26.
108. J. Ellis and K. A. Olive, *Phys. Lett.* 193B (1987) 525; R. M. Ayale, J. Wilson, J. Ellis, K. A. Olive, D. N. Schramm, and G. Steigman, *Phys. Lett.* 203B (1988) 188; 219B (1989) 515; G. Racliet and D. Seckel, *Phys. Rev. Lett.* 60 (1988) 1793; 67 (1991) 2605; A. Burrows, T. Ressel, and M. S. Turner, *Phys. Rev. D* 42 (1990) 1020; W. Keil, H. T. Janka, D. N. Schramm, G. Sigl, M. S. Turner and J. R. Ellis, *Phys. Rev. D* 56 (1997) 2419.
109. J. Wess and J. Bagger, *Supersymmetry and Supergravity*, Princeton University Press, Princeton NJ, 1992); G. G. Ross, *Grand Unified Theories*, Addison-Wesley, Redwood City CA, 1985); S. Martin, [arXiv:hep-ph/9709356](#); J. Ellis, [arXiv:hep-ph/9812235](#); K. A. Olive, [arXiv:hep-ph/9911307](#).
110. L. M. Aiani, *Proceedings of the 1979 Gif-sur-Yvette Summer School on Particle Physics*, 1; G. 't Hooft, in *Recent Developments in Gauge Theories*, Proceedings of the Nato Advanced Study Institute, Cargese, 1979, eds. G. 't Hooft et al., (Plenum Press, NY, 1980); E. Witten, *Phys. Lett.* B 105, 267 (1981).
111. J. Ellis, J. S. Hagelin, D. V. Nanopoulos, K. A. Olive and M. Srednicki, *Nucl. Phys. B* 238 (1984) 453; see also H. G. Goldberg, *Phys. Rev. Lett.* 50 (1983) 1419.
112. J. Rich, M. Spiro and J. Lloyd-Owen, *Phys. Rep.* 151 (1987) 239; P. F. Smith, *Contemp. Phys.* 29 (1998) 159; T. K. Hemmick et al., *Phys. Rev. D* 41 (1990) 2074.
113. L. E. Ibanez, *Phys. Lett.* 137B (1984) 160; J. Hagelin, G. L. Kane, and S. Raby, *Nucl. Phys. B* 241 (1984) 638; T. Falk, K. A. Olive, and M. Srednicki, *Phys. Lett. B* 339 (1994) 248 [[arXiv:hep-ph/9409270](#)].
114. see e.g. K. A. Olive and M. Srednicki, *Phys. Lett.* 205B (1988) 553.
115. The LEP Collaborations, the LEP Electroweak Working Group, and the SLD Heavy Flavour and Electroweak Groups, CERN-EP-2000-016.
116. L. E. Ibanez and G. G. Ross, *Phys. Lett. B* 110 (1982) 215; L. E. Ibanez, *Phys. Lett. B* 118 (1982) 73; J. Ellis, D. V. Nanopoulos and K. Tamvakis, *Phys. Lett. B* 121 (1983) 123; J. Ellis, J. Hagelin, D. V. Nanopoulos and K. Tamvakis, *Phys. Lett. B* 125 (1983) 275; L. Alvarez-Gaume, J. Polchinski, and M. Wise, *Nucl. Phys. B* 221 (1983) 495.

117. K A . O live and M . Srednicki, Phys. Lett. B 230, 78 (1989); Nucl. Phys. B 355 (1991) 208.

118. A LEPH collaboration, D . D ecam p et al, Phys. Rep. 216 (1992) 253; L3 collaboration, M . A cciarri et al, Phys. Lett. B 350 (1995) 109; O P A L collaboration, G . A lexander et al, Phys. Lett. B 377 (1996) 273.

119. Joint LEP 2 Supersymmetry Working Group, Combined LEP Chargino Results, up to 208 GeV,  
[http://lepsusy.web.cern.ch/lepsusy/www/inos\\_moriond01/charginos\\_pub.html](http://lepsusy.web.cern.ch/lepsusy/www/inos_moriond01/charginos_pub.html).

120. K . G riest and D . Seckel, Phys. Rev. D 43 (1991) 3191.

121. J. Ellis, T. Falk, and K A . O live, Phys. Lett. B 444 (1998) 367 [[arXiv:hep-ph/9810360](http://arXiv:hep-ph/9810360)]; J. Ellis, T. Falk, K A . O live, and M . Srednicki, Astr. Part. Phys. 13 (2000) 181 [Erratum -ibid. 15 (2001) 413] [[arXiv:hep-ph/9905481](http://arXiv:hep-ph/9905481)].

122. M . E . G om ez, G . Lazarides and C. Pallis, Phys. Rev. D 61 (2000) 123512 [[arXiv:hep-ph/9907261](http://arXiv:hep-ph/9907261)]; Phys. Lett. B 487 (2000) 313 [[arXiv:hep-ph/0004028](http://arXiv:hep-ph/0004028)]; Nucl. Phys. B 638 (2002) 165 [[arXiv:hep-ph/0203131](http://arXiv:hep-ph/0203131)]; R . A mow itt, B . D utta and Y . Santoso, Nucl. Phys. B 606 (2001) 59; T . N ihei, L . R oszkowski and R . R uiz de A ustri, JHEP 0207 (2002) 024 [[arXiv:hep-ph/0206266](http://arXiv:hep-ph/0206266)].

123. C . Boehm , A . D juadi and M . D rees, Phys. Rev. D 62 (2000) 035012; J. Ellis, K A . O live and Y . Santoso, Astropart. Phys. 18 (2003) 395 [[arXiv:hep-ph/0112113](http://arXiv:hep-ph/0112113)].

124. M . D rees and M . M . N ojiri, Phys. Rev. D 47 (1993) 376; H . Baer and M . B rhlík, Phys. Rev. D 53 (1996) 59; and Phys. Rev. D 57 (1998) 567; H . Baer, M . B rhlík, M . A . D iaz, J. Ferrandis, P . M ercadante, P . Q uintana and X . Tata, Phys. Rev. D 63 (2001) 015007; A . B . Lahanas, D . V . N anopoulos and V . C . Spanos, Mod. Phys. Lett. A 16 (2001) 1229.

125. J. R . E llis, T . Falk, G . G anis, K . A . O live and M . Srednicki, Phys. Lett. B 510 (2001) 236 [[arXiv:hep-ph/0102098](http://arXiv:hep-ph/0102098)].

126. J. L. Feng, K . T . M atchev and T . M oroi, Phys. Rev. Lett. 84 (2000) 2322; J. L. Feng, K . T . M atchev and T . M oroi, Phys. Rev. D 61 (2000) 075005; J. L. Feng, K . T . M atchev and F . W ilczek, Phys. Lett. B 482 (2000) 388.

127. M . B attaglia et al, Eur. Phys. J. C 22 (2001) 535 [[arXiv:hep-ph/0106204](http://arXiv:hep-ph/0106204)]; see also: B . C . A llanach et al, in Proc. of the APS/DPF/DPB Summer Study on the Future of Particle Physics (Snowmass 2001) ed. N . G raf, Eur. Phys. J. C 25 (2002) 113 [[arXiv:hep-ph/0202233](http://arXiv:hep-ph/0202233)].

128. LEP Higgs Working Group for Higgs boson searches, O P A L Collaboration, A LEPH Collaboration, D E LPH I Collaboration and L3 Collaboration, Search for the Standard Model Higgs Boson at LEP , A LEPH -2001-066, D E LPH I-2001-113, CERN -L3-NOTE-2699, O P A L-PN -479, LHW G -NOTE -2001-03, CERN -EP /2001-055, [arXiv:hep-ex/0107029](http://arXiv:hep-ex/0107029); Searches for the neutral Higgs bosons of the M SSM : Preliminary combined results using LEP data collected at energies up to 209 GeV , LHW G -NOTE -2001-04, A LEPH -2001-057, D E LPH I-2001-114, L3-NOTE -2700, O P A L-TN -699, [arXiv:hep-ex/0107030](http://arXiv:hep-ex/0107030); LHW G Note/2002-01,  
[http://lephiggs.web.cern.ch/LEPHIGGS/papers/July2002\\_SM/index.html](http://lephiggs.web.cern.ch/LEPHIGGS/papers/July2002_SM/index.html).

129. M.S. Alam et al, [CLEO Collaboration], *Phys. Rev. Lett.* 74 (1995) 2885 as updated in S. Ahmed et al, CLEO CONF 99-10; BELLE Collaboration, BELLE-CONF-0003, contribution to the 30th International conference on High-Energy Physics, Osaka, 2000; See also K. Abe et al, [Belle Collaboration], [[arX iv:hep-ex/0107065](#)]; L. Lista [BaBar Collaboration], [[arX iv:hep-ex/0110010](#)]; K. Chetyrkin, M. Misiak and M. Münz, *Phys. Lett. B* 400 (1997) 206 [Erratum -*ibid. B* 425 (1997) 414] [[hep-ph/9612313](#)]; T. Hurth, [hep-ph/0106050](#); C. Degrassi, P. Gambino and G. F. Giudice, *JHEP* 0012 (2000) 009; M. Carena, D. Garcia, U. Nierste and C. E. Wagner, *Phys. Lett. B* 499 (2001) 141; P. Gambino and M. Misiak, *Nucl. Phys. B* 611 (2001) 338; D. A. Demir and K. A. Olive, *Phys. Rev. D* 65 (2002) 034007.

130. H.N. Brown et al. [Muon g-2 Collaboration], *Phys. Rev. Lett.* 86 (2001) 2227.

131. M. Nech and A. Nyeler, *Phys. Rev. D* 65 (2002) 073034; M. Nech, A. Nyeler, M. Perrottet and E. De Rafael, *Phys. Rev. Lett.* 88 (2002) 071802; M. Hayakawa and T. Kinoshita, [[arX iv:hep-ph/0112102](#)]; I. Blokland, A. Czarnecki and K. Melnikov, *Phys. Rev. Lett.* 88 (2002) 071803; J. Bijnens, E. Pallante and J. Prades, *Nucl. Phys. B* 626 (2002) 410.

132. G.W. Bennett et al. [Muon g-2 Collaboration], *Phys. Rev. Lett.* 89 (2002) 101804 [Erratum -*ibid. B* 89 (2002) 129903] [[arX iv:hep-ex/0208001](#)].

133. M. Davier, S. Eidelman, A. Hocker and Z. Zhang, [[arX iv:hep-ph/0208177](#)]; see also K. Hagiwara, A. D. Martin, D. Nomura and T. Teubner, [[arX iv:hep-ph/0209187](#)]; F. Jegerlehner (unpublished, as reported in M. Krawczyk, *Acta Phys. Polon. B* 33 (2002) 2621 [[arX iv:hep-ph/0208076](#)]).

134. J. R. Ellis, K. A. Olive and Y. Santoso, *New Jour. Phys.* 4 (2002) 32 [[arX iv:hep-ph/0202110](#)].

135. Joint LEP 2 Supersymmetry Working Group, Combined LEP Selettron/Muon/Stau Results, 183-208 GeV,  
[http://alephwww.cern.ch/~ganis/SUSYWG/SLEP/sleptons\\_2k01.html](http://alephwww.cern.ch/~ganis/SUSYWG/SLEP/sleptons_2k01.html).

136. A. B. Lahanas, D. V. Nanopoulos and V. C. Spanos, *Phys. Lett. B* 518 (2001) 94 [[arX iv:hep-ph/0107151](#)]; V. Barger and C. Kao, *Phys. Lett. B* 518 (2001) 117 [[arX iv:hep-ph/0106189](#)]; L. Roszkowski, R. Ruiz de Austri and T. Nishi, *JHEP* 0108 (2001) 024 [[arX iv:hep-ph/0106334](#)]; A. Djouadi, M. Drees and J. L. Kneur, *JHEP* 0108 (2001) 055 [[arX iv:hep-ph/0107316](#)]; H. Baer, C. Balazs and A. Belyaev, *JHEP* 0203 (2002) 042 [[arX iv:hep-ph/0202076](#)].

137. S. Heinemeyer, W. Hollik and G. Weiglein, *Comput. Phys. Commun.* 124 (2000) 76 [[arX iv:hep-ph/9812320](#)]; S. Heinemeyer, W. Hollik and G. Weiglein, *Eur. Phys. J. C* 9 (1999) 343 [[arX iv:hep-ph/9812472](#)]. M. Frank, S. Heinemeyer, W. Hollik and G. Weiglein, [[arX iv:hep-ph/0202166](#)].

138. L.L. Everett, G.L. Kane, S. Rigolin and L. Wang, *Phys. Rev. Lett.* 86 (2001) 3484; J.L. Feng and K.T.M. Matchev, *Phys. Rev. Lett.* 86 (2001) 3480; E.A. Baltz and P.G.ondolo, *Phys. Rev. Lett.* 86 (2001) 5004; U. Chattopadhyay and P.N. Nath, *Phys. Rev. Lett.* 86 (2001) 5854; S. Komine, T.M. Orio and M. Yamaguchi, *Phys. Lett. B* 506 (2001) 93; J. Ellis, D.V. Nanopoulos and

K . A . O live, Phys. Lett. B 508 (2001) 65; R . A mow itt, B . Dutta, B . Hu and Y . Santoso, Phys. Lett. B 505 (2001) 177; S . P . M artin and J . D . W ells, Phys. Rev. D 64 (2001) 035003; H . Baer, C . Balazs, J . Ferrandis and X . Tata, Phys. Rev. D 64 (2001) 035004.

139. M . D rees, M . M . N o jiri, D . P . Roy and Y . Yam ada, Phys. Rev. D 56 (1997) 276 [Erratum -ibid. D 64 (1997) 039901] [[arX iv:hep-ph/9701219](https://arxiv.org/abs/hep-ph/9701219)]; M . D rees, Y . G . K im, M . M . N o jiri, D . T oya, K . H asuko and T . K obayashi, Phys. Rev. D 63 (2001) 035008 [[arX iv:hep-ph/0007202](https://arxiv.org/abs/hep-ph/0007202)]. V . Berezinsky, A . Bottino, J . R . Ellis, N . Fomengo, G . M ignola and S . Scopel, A stropart. Phys. 5 (1996) 1 [[arX iv:hep-ph/9508249](https://arxiv.org/abs/hep-ph/9508249)]; P . N ath and R . A mow itt, Phys. Rev. D 56 (1997) 2820 [[arX iv:hep-ph/9701301](https://arxiv.org/abs/hep-ph/9701301)]; A . Bottino, F . D onato, N . Fomengo and S . Scopel, Phys. Rev. D 63 (2001) 125003 [[arX iv:hep-ph/0010203](https://arxiv.org/abs/hep-ph/0010203)]; V . Bertin, E . Nezri and J . O rlo , [arX iv:hep-ph/0210034](https://arxiv.org/abs/hep-ph/0210034).

140. J . Ellis, K . O live and Y . Santoso, Phys. Lett. B 539 (2002) 107 [[arX iv:hep-ph/0204192](https://arxiv.org/abs/hep-ph/0204192)]; J . R . Ellis, T . Falk, K . A . O live and Y . Santoso, [arX iv:hep-ph/0210205](https://arxiv.org/abs/hep-ph/0210205).

141. J . R . Ellis, A . Ferstl and K . A . O live, Phys. Lett. B 532 (2002) 318 [[arX iv:hep-ph/0111064](https://arxiv.org/abs/hep-ph/0111064)].

142. J . R . Ellis, A . Ferstl and K . A . O live, Phys. Lett. 481 (2000) 304 [[arX iv:hep-ph/0001005](https://arxiv.org/abs/hep-ph/0001005)].

143. J . R . Ellis, A . Ferstl and K . A . O live, Phys. Rev. D 63 (2001) 065016 [[arX iv:hep-ph/0007113](https://arxiv.org/abs/hep-ph/0007113)].

144. J . R . Ellis and K . A . O live, Phys. Lett. B 514 (2001) 114 [[arX iv:hep-ph/0105004](https://arxiv.org/abs/hep-ph/0105004)].

145. D . Abram s et al. [CDM S Collaboration], Phys. Rev. D 66 (2002) 122003 [[arX iv:astro-ph/0203500](https://arxiv.org/abs/astro-ph/0203500)].

146. A . Benoit et al, Phys. Lett. B 545 (2002) 43 [[arX iv:astro-ph/0206271](https://arxiv.org/abs/astro-ph/0206271)].

147. DAM A Collaboration, R . Bernabeu et al, Phys. Lett. B 436 (1998) 379.

148. E . A ccom ando, R . A mow itt, B . Dutta and Y . Santoso, Nucl. Phys. B 585 (2000) 124 [[arX iv:hep-ph/0001019](https://arxiv.org/abs/hep-ph/0001019)]; A . Bottino, F . D onato, N . Fomengo and S . Scopel, Phys. Rev. D 63 (2001) 125003 [[arX iv:hep-ph/0010203](https://arxiv.org/abs/hep-ph/0010203)]; M . D rees, Y . G . K im, T . K obayashi and M . M . N o jiri, Phys. Rev. D 63 (2001) 115009 [[arX iv:hep-ph/0011359](https://arxiv.org/abs/hep-ph/0011359)]; Y . G . K im and M . M . N o jiri, Prog. Theor. Phys. 106 (2001) 561 [[arX iv:hep-ph/0104258](https://arxiv.org/abs/hep-ph/0104258)]. A . B . Lahanas, D . V . N anopoulos and V . C . Spanos, Mod. Phys. Lett. A 16 (2001) 1229 [[arX iv:hep-ph/0009065](https://arxiv.org/abs/hep-ph/0009065)]; A . B . Lahanas, D . V . N anopoulos and V . C . Spanos, Phys. Lett. B 518 (2001) 94 [[arX iv:hep-ph/0107151](https://arxiv.org/abs/hep-ph/0107151)]. M . E . G om ez and J . D . Vergados, Phys. Lett. 512 (2001) 252 [[arX iv:hep-ph/0012020](https://arxiv.org/abs/hep-ph/0012020)].

149. J . Ellis, J . L . Feng, A . Ferstl, K . T . M atchev and K . A . O live, Eur. Phys. J. C 24 (2002) 311 [[arX iv:astro-ph/0110225](https://arxiv.org/abs/astro-ph/0110225)].

150. CDM S Collaboration, R . W . Schnee et al, Phys. Rep. 307 (1998) 283.

151. CRESST Collaboration, M . Br avin et al, A stropart. Phys. 12 (1999) 107.

152. H . V . K lapdor-K leingrothaus, [arX iv:hep-ph/0104028](https://arxiv.org/abs/hep-ph/0104028).

153. G . Jungm an, M . K am ionkow ski and K . G riest, Phys. Rep. 267 (1996) 195; <http://t8web.lanl.gov/people/jungman/neut-package.html> .